Petroleum Science 22 (2025) 3069–3085

Contents lists available at ScienceDirect

Petroleum Science

journal homepage: www.keaipublishing.com/en/journals/petroleum-science

Original Paper

The genesis and accumulation mechanism of CBM in the typical mid- to low-rank coal-bearing basins

Bin Zhang [a,b], Shu Tao [a,b,*], Fan Yang [c,**], Yi Cui [d], Qing-He Jing [d], Jie Guo [d], Shi-Da Chen [a,b], Yi-Jie Wen [a,b], Xin-Yang Men [a,b]

[a] School of Energy Resources, China University of Geosciences (Beijing), Beijing, 100083, China
[b] Coal Reservoir Laboratory of National Engineering Research Center of CBM Development & Utilization, Beijing, 100083, China
[c] PetroChina Research Institute of Petroleum Exploration and Development, Beijing, 100083, China
[d] Zhalainuoer Coal Industry Co., Ltd., Hulunbuir, 021410, Inner Mongolia, China

ARTICLE INFO

Article history:
Received 6 September 2024
Received in revised form
14 March 2025
Accepted 16 April 2025
Available online 17 April 2025

Edited by Jie Hao

Keywords:
Coalbed methane
Biogenic gas
Isotope geochemistry
Migration-accumulation model
Mid- to low-rank coal

ABSTRACT

The composition and isotopic characteristics of coalbed methane (CBM), as well as the genesis of CH_4 and CO_2, associated geological process and migration-accumulation model of CBM in typical mid- to low-rank coal-bearing basins were studied. The genesis of CBM is jointly influenced by the degree of coalification and biochemical processes, which in turn determine the composition and isotopic characteristics of CBM. Biogenic gas is extensively developed in mid- to low-rank coal-bearing basins, but its genesis varies. In the Baode area, China, and the San Juan Basin, USA, CBM is mainly secondary biogenic gas and thermogenic gas. In the Miquan area, China, CBM is characterized by primary biogenic gas. However, CBM in the Jiergalangtu area, China, Surat Basin, Australia, and Power River Basin, USA, are characterized by secondary biogenic gas. Microbial CO_2 reduction occurs in these coal-bearing basins, but with significant gas generation by acetate fermentation in some areas of these basins. Moreover, CO_2 in the Power River Basin, Surat Basin, and Jiergalangtu area mainly originates from microbial degradation of organic matter. However, in other basins studied, CO_2 initially derives from coal pyrolysis and is subsequently supplemented by CO_2 from microbial methanogenesis. The generation and isotope fractionation of CBM are affected and controlled by associated geological processes. Additionally, under the control of tectonic morphology and hydrogeological conditions, the genesis and migration-accumulation models of CBM in mid- to low-rank coal-bearing basins can be summarized into two models—the hydrodynamic active monoclinic model and the hydrodynamic differential syncline model—or a combination of the two.

1. Introduction

Coalbed methane (CBM) is a crucial source of unconventional clean energy, and its development and utilization have positive significance for alleviating energy crisis, improving atmospheric environment and reducing coal mine disasters (Bates et al., 2011; Ma et al., 2022; Zhang et al., 2023; Liu et al., 2024). The geological resources of CBM in China below 2000 m can reach 29.8×10^{12} m^3. Among them, the geological resources of mid- to low-rank CBM are about 19.5×10^{12} m^3 (Tao et al., 2019a), mainly in the Junggar Basin, the eastern margin of the Ordos Basin, and the Erlian Basin (Qin et al., 2017; Tao et al., 2019b). The classification standard of vitrinite reflectance (R_o) of the mid- to low-rank coals is based on Xu et al. (2019) (low-rank coals are 0.5%–0.8% R_o, mid-rank coals are 0.8%–1.3% R_o). With the successful development of CBM in the mid- to low-rank coal-bearing basins, such as the San Juan Basin and Powder River Basin in the United States, the Alberta Basin in Canada, and the Surat Basin in Australia, China has paid more attention to the exploration and development of CBM in the mid- to low-rank coals (Xu et al., 2015; Tao et al., 2017, 2018; Zhang et al., 2024). However, currently, large-scale CBM development in China is primarily concentrated in high-rank coals areas, such as the southern Qinshui Basin, while exploration and development in mid- to low-rank coals remain in the early stages (Tao et al., 2012; Chen et al.,

* Corresponding author.
** Corresponding author.
E-mail addresses: taoshu@cugb.edu.cn (S. Tao), yangfan84@foxmail.com (F. Yang).
Peer review under the responsibility of China University of Petroleum (Beijing).

https://doi.org/10.1016/j.petsci.2025.04.017
1995-8226/

2015; Zhang et al., 2022). Because CBM in the mid- to low-rank coals is different from that in high-rank coals in many aspects, such as genetic type, occurrence state, and reservoir conditions (Ye et al., 2022; Wu et al., 2023; Ma et al., 2024), it is necessary to carry out a systematic comparative study on the genesis and migration-accumulation models of CBM in the mid- to low-rank coals in some typical coal-bearing basins.

The volume fractions of CH_4 and CO_2, along with their carbon and hydrogen isotopes in CBM, contain extensive geological and geochemical information (Whiticar, 1999; Ayers, 2002; Tang et al., 2022; Zhang et al., 2024). Therefore, the composition and isotopic parameters or their ratios are widely used to determine the genesis and generation pathways of CH_4 and CO_2, such as $C_1/(C_2+C_3)$ (the number denotes the number of carbon atoms), $\delta^{13}C(CH_4)$ versus $\delta D(CH_4)$, $\delta^{13}C(CH_4)$ versus CDMI [(CDMI = $CO_2/(CO_2+CH_4)$], etc (Kvenvolden, 1995; Whiticar, 1999; Boreham and Edwards, 2008; Bates et al., 2011; Hamilton et al., 2014). Specifically, microbial degradation can significantly reduce $\delta^{13}C(CH_4)$, but different microbial fermentation methods have different effects on $\delta^{13}C(CH_4)$. The value of $\delta^{13}C(CH_4)$ affected by acetate fermentation ranges from −65‰ to −50‰, while the value of $\delta^{13}C(CH_4)$ produced by CO_2 reduction ranges from −110‰ to −65‰ (Tang et al., 2022). CO_2 is usually a secondary component in CBM, which mainly comes from pyrolysis and microbial degradation in the early stage of coalification. Compared with biogenic gas, the $\delta^{13}C(CH_4)$ of thermogenic gas is obviously heavier, ranging from −50‰ to −20‰ (Tang et al., 2022). The $\delta^{13}C(CO_2)$ values resulting from pyrolysis range from −25‰ to −5‰, whereas those from microbial action range from −40‰ to 20‰ (Clayton, 1998). Milkov and Etiope (2018) revised these gas genetic cross plots, suggesting that the thermogenic gas field should be expanded to include both early mature gas ($\delta^{13}C(CH_4)$ as low as −75‰) and late mature gas ($\delta^{13}C(CH_4)$ approximately −15‰). Additionally, the revised gas genetic cross plots by Milkov and Etiope (2018) effectively distinguish between primary biogenic gas and secondary biogenic gas.

The genesis of CBM in the mid- to low-rank coals is complex. Previous gas genetic cross plots were limited by the number of sample points, which may impose certain restrictions on determining the genesis of CBM. Therefore, a new gas genetic cross plot from Milkov and Etiope (2018) was employed to reassess gas genesis. Additionally, combined with the actual geological conditions, such as hydrodynamic conditions and structural morphology, provides a more comprehensive analysis of the genesis and migration-accumulation of CBM. This study systematically analyzes the genesis and migration-accumulation models of CBM in the Baode (BD) area on the eastern margin of the Ordos Basin and the Jiergalangtu (JL) area in the Erlian Basin. Additionally, to better understand the CBM genesis and migration-accumulation models in mid- to low-rank coals, the study also includes comparative analysis using CBM data from other typical coal-bearing basins. Moreover, the geological processes related to CBM genesis and isotope fractionation are discussed to provide deeper insights into the processes influencing changes in gas composition and isotopic characteristics.

2. Methods

2.1. Gas composition and stable isotope tests

45 CBM samples were collected from the BD area (0.52%–0.89% R_o), 16 CBM samples were collected from the JL area (0.28%–0.6% R_o). In total, 61 CBM samples were obtained from the wellheads of production wells using the drainage gas gathering method and were stored in 1 L aluminum foil bags. The sample locations are shown in Figs. 1(d) and 2. All gas samples were analyzed for $\delta^{13}C(CH_4)$, $\delta^{13}C(CO_2)$, $\delta D(CH_4)$, and gas composition (Table 1). Gaseous isotopes were measured using a MAT253 stable isotope ratio mass spectrometer, while gas compositions were analyzed with an Agilent GC 7890A gas chromatograph. Carbon and hydrogen isotope analyses adhered to Vienna Pee Dee Belemnite (VPDB) and Vienna Standard Mean Ocean Water (VSMOW) standards, respectively, with an experimental precision of ±0.2‰. Detailed operating procedures for these experiments are described in Dai et al. (2012) and Zhang et al. (2020).

2.2. Coal pyrolysis tests

In order to analyze the change of volume fraction of CH_4 and CO_2 during coalification, the coal samples from the JL area and BD area were collected (0.35% R_o and 0.62% R_o, respectively) for thermal simulation experiments. This experiment was conducted using a high-temperature, high-pressure pyrolysis apparatus. The pressure of the experimental system was set to 50 MPa, and the temperature was increased at a heating rate of 30 °C/h. The experimental temperatures were set at 240, 270, 300, 330, 360, 390, 420, 450, 480, 510, 540, 570, and 600 °C, respectively. In this experiment, the gas components at various temperatures were measured to examine the changes in CH_4 and CO_2 contents during thermal evolution.

2.3. Data collection of CBM in typical basins

In addition to the 61 CBM samples analyzed in this study, composition and isotope data from CBM in typical mid- to low-rank coal-bearing basins around the world were systematically collected for comparative analysis (Table 2). This dataset includes 15 samples from the Miquan (MQ) area (<0.5% R_o) in the southern margin of the Junggar Basin (Li et al., 2021a), 20 samples from the Powder River (PR) Basin (0.31%–0.49% R_o) (Flores et al., 2008), 26 samples from the San Juan (SJ) Basin (0.7%–1.5% R_o) (Zhou et al., 2005) in the United States, and 16 samples from Surat (SR) Basin (0.35%–0.7% Ro) in Australia (Hamilton et al., 2014).

3. Results

3.1. CBM composition

Although CH_4 is the main composition of CBM, its volume fraction varies greatly in different basins. As show in Tables 1–3, the SR Basin has the highest CH_4 volume fraction (94.6%–99.5%, mean: 98.8%), followed by the BD area (84.4%–93.1%, mean: 88.00%), the PR Basin (70.06%–97.95%, mean: 87.25%), the SJ Basin (81.37%–93.17%, mean: 86.7%), and the MQ area (54.12%–97.95%, mean: 77.62%), while the JL area has the lowest CH_4 volume fraction (26.82%–91.25%, mean: 55.76%).

In addition, the volume fraction of non-hydrocarbon gases also varies greatly among different basins (Tables 1–3). The MQ area, SJ Basin, and PR Basin show high abnormal CO_2 volume fraction characteristics. The variation range of CO_2 volume fraction in the MQ area is the largest (0.86%–44.84%), followed by the PR Basin (0.9%–28.81%) and the SJ Basin (0.07%–18.01%). The CO_2 volume fraction in the BD area and the JL area is close, ranging from 1.8% to 12.5% and 0.82%–9.96%, respectively. The SR Basin has the smallest variation of CO_2 volume fraction, ranging from 0.44% to 1.12%. As shown in Fig. 3, the volume fraction of CO_2 in the BD area, MQ area, PR Basin, and JL area gradually increases with burial depth. The volume fraction of N_2 also varies widely among different basins (Tables 1–3). The range of N_2 volume fraction in the JL area is the largest, ranging from 7.93% to 71.19%, followed by the BD area, MQ area, and PR Basin, ranging from 1.4% to 11.8%, 0%–14.33% and 0%–7.83%, respectively. The SR Basin and SJ Basin has the smallest

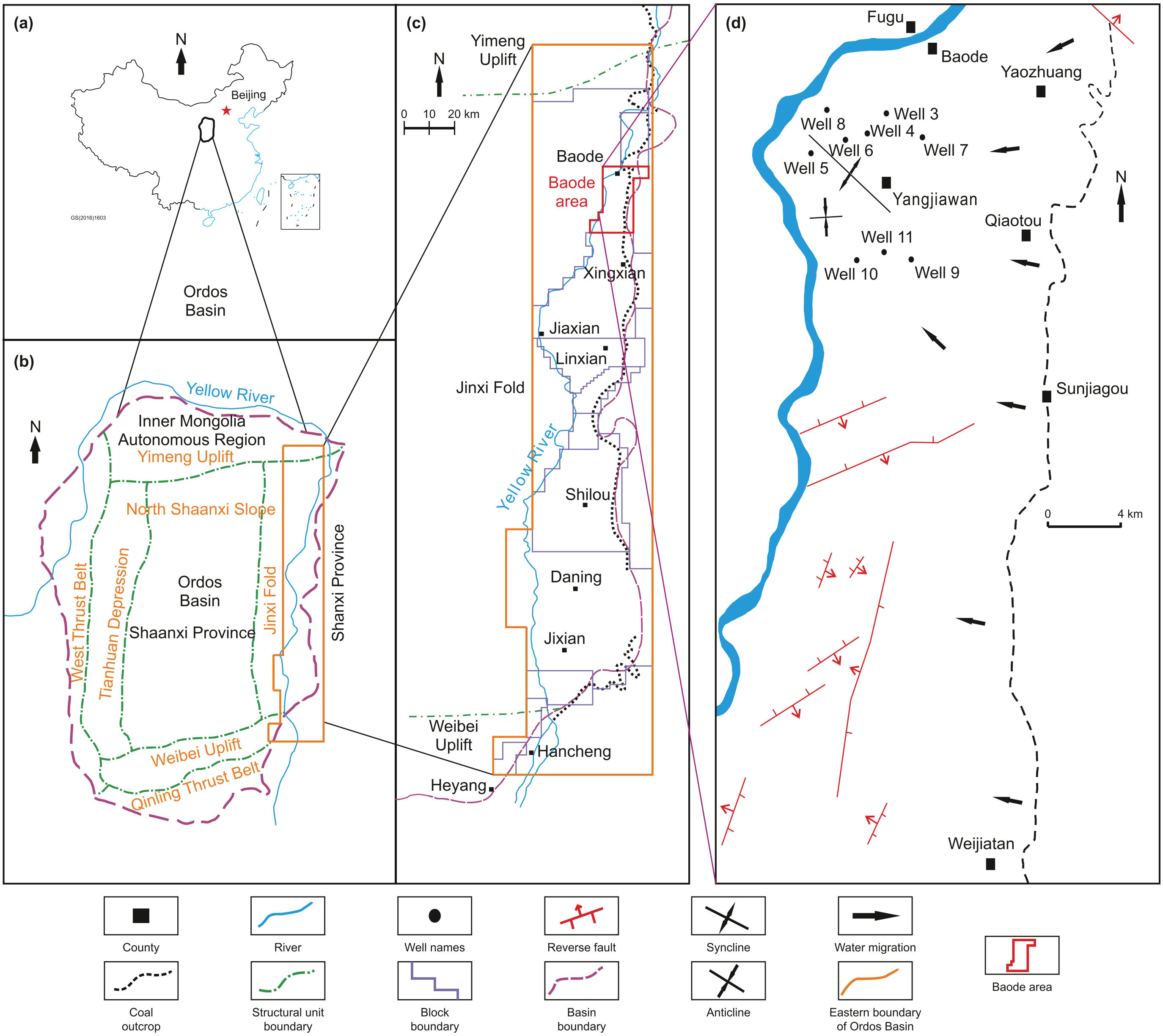

Fig. 1. (**a**) Schematic map shows the outline of China; (**b**) Tectonic sketch map of the Ordos Basin in China; (**c**) The regional location map of BD area is on the eastern margin of Ordos Basin; (**d**) Map of the BD area shows the locations of 11 CBM wells sampled in this study.

variation of N_2 volume fraction, ranging from 0% to 4.18% and 0%–1.21%.

3.2. CBM isotope

The $\delta^{13}C(CH_4)$ and $\delta D(CH_4)$ typically exhibit significant negative values (Tables 1–3). These isotopic values vary substantially across different basins. In the BD area, $\delta^{13}C(CH_4)$ ranges from −45.7‰ to −61.8‰ (mean: 52.6‰), and $\delta D(CH_4)$ ranges from −242.4‰ to −259.4‰ (mean: 248.8‰), indicating a mixed origin for CH_4. In the PR Basin, $\delta^{13}C(CH_4)$ ranges from −49.2‰ to −81.53‰ (mean: 62.5‰), and $\delta D(CH_4)$ ranges from −321.7‰ to −290.2‰ (mean: 307.91‰), reflecting obvious microbial genetic characteristics. Similar isotopic characteristics are observed in the JL area and SR Basin. In the JL area, $\delta^{13}C(CH_4)$ ranges from −50.3‰ to −61.7‰ (mean: 57.8‰), and $\delta D(CH_4)$ ranges from −241‰ to −285‰ (mean: 278‰). In the SR Basin, $\delta^{13}C(CH_4)$ ranges from −45.3‰ to −54.5‰ (mean: 49.7‰), and $\delta D(CH_4)$ ranges from −213‰ to −236‰ (mean: 220‰). The MQ area shows the largest negative values, with $\delta^{13}C(CH_4)$ ranging from −52.05‰ to −77.79‰ (mean: 66.14‰), and $\delta D(CH_4)$ ranging from −226.37‰ to −274.29‰ (mean: 253.84‰), preliminarily showing the biogenic characteristics. Conversely, the isotopes of CH_4 in the SJ Basin have the least negative values, with $\delta^{13}C(CH_4)$ ranging from −42.43‰ to −47.87‰ (mean: 44.13‰) and $\delta D(CH_4)$ ranging from −196.6‰ to −247.1‰ (mean: 211.3‰), suggesting thermogenic characteristics.

The distribution of $\delta^{13}C(CO_2)$ values varies significantly across different basins. Fig. 4 shows that $\delta^{13}C(CO_2)$ values of all samples range from −25.8‰ to 18.16‰. Among these, the $\delta^{13}C(CO_2)$ values in the PR Basin exhibit the largest range between positive and negative values (from −24.6‰ to 14.1‰), followed by the SJ Basin (from −12.65‰ to 18.16‰), the BD area (from −10.5‰ to 13.9‰),

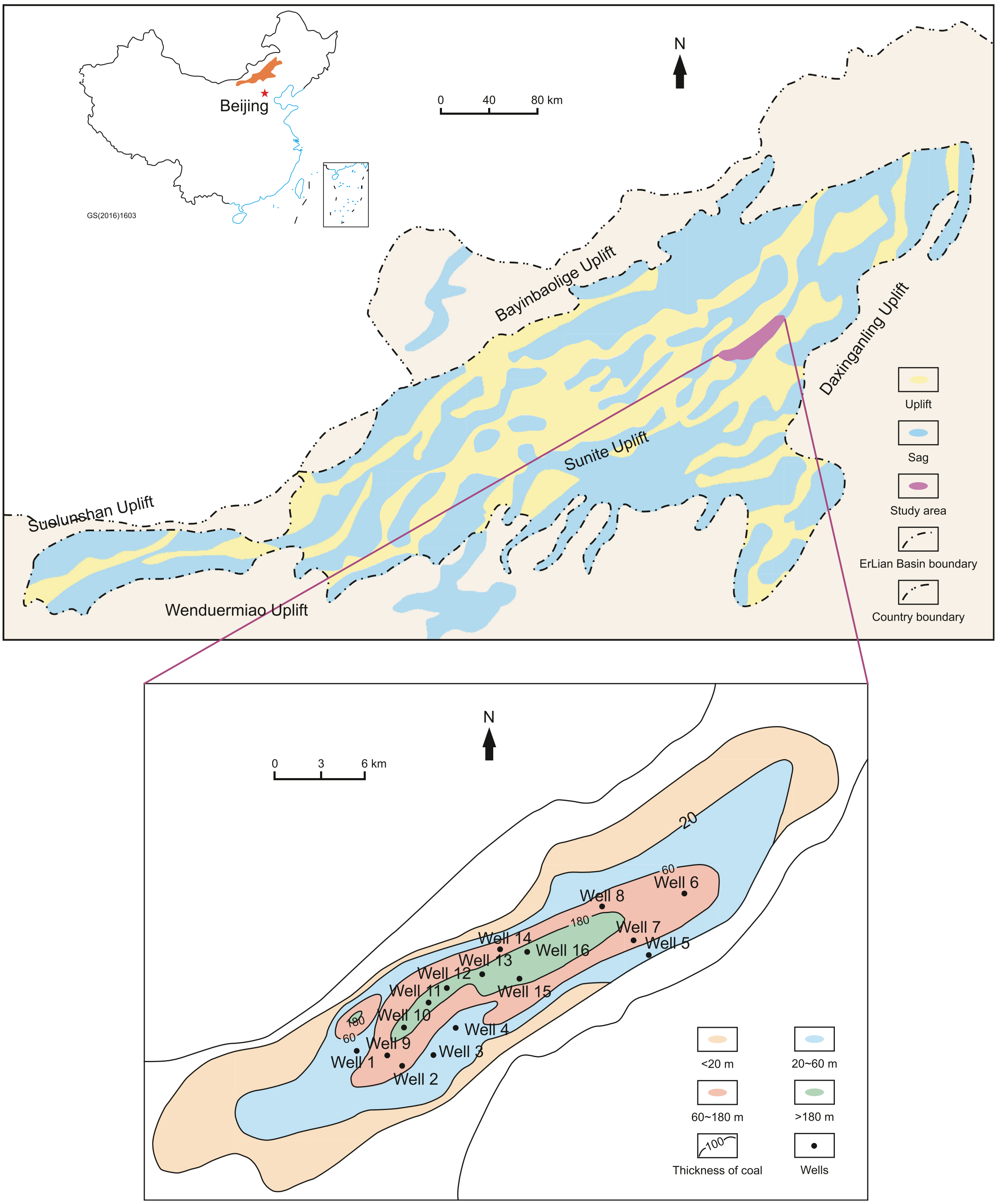

Fig. 2. Map of the JL area showing locations of 16 CBM wells sampled in this study (modified from Sun et al. (2018) and Ma et al. (2023)).

Table 1
The composition and isotope values of CBM in the BD and JL areas in China.

Area	Well name	Depth, m	Sample No.	$\delta^{13}C$, ‰		δD, ‰	Gas volume fraction, %				$C_1/(C_2+C_3)$
				CH_4	CO_2		CH_4	CO_2	N_2	C_2+C_3	
BD	Well 1	501	B1-1	−55	−7.2	−253.7	89.6	2.7	7.4	0.3	299
		503	B1-2	−55.3	−8.7	−255.6	85.0	3.3	11.8	-	-
		546	B1-3	−61.8	−9.8	−259.4	91.6	4.4	4.1	-	-
		547	B1-4	−61.4	−10.5	−259.3	87.6	3.0	9.4	-	-
	Well 2	1011	B2-1	−51.2	−3.1	−242.5	93.1	3.7	3.3	-	-
		1015	B2-2	−48.6	−3.7	−245.8	90.3	3.0	6.3	0.34	266
		1061	B2-3	−51.1	3.6	−250.9	88.2	9.0	2.6	0.16	551
		1064	B2-4	−51.4	5.5	−249.4	87.2	10.8	1.8	0.18	484
		1066	B2-5	−51.2	5.0	−250.4	87.7	10.3	1.6	0.4	219
		1067	B2-6	−51.4	5.3	−249.2	84.4	11.2	2.2	2.2	38
		1068	B2-7	−50.8	5.0	−248.6	86.8	8.4	1.5	3.3	26
	Well 3	622.00	B3-1	−54.1	10.3	−251.6	89.6	3.8	6.2	0.4	224
		624.00	B3-2	−54.1	10.2	−253.3	90.3	3.5	6	0.2	451
	Well 4	866.00	B4-1	−51.4	12.8	−252.6	86.3	11	2.5	0.2	431
		870.00	B4-2	−51.5	13.1	−249.6	86.6	10.6	2.2	0.6	144
	Well 5	880.00	B5-1	−51.3	10.3	−243.2	85.0	11.3	3.2	0.5	170
		883.00	B5-2	−51.6	10.4	−242.4	85.5	11.6	2.8	0.1	855
	Well 6	810.00	B6-1	−51.6	11.7	−246.1	88.0	8.8	2.5	0.7	126
		816.00	B6-2	−51.8	11.5	−245.7	87.5	10.1	2	0.4	219
	Well 7	728.00	B7-1	−53.4	12.2	−249.5	91.2	4.2	4.2	0.4	228
		730.00	B7-2	−53.7	12.1	−250.1	89.9	1.8	8	0.3	300
	Well 8	872.00	B8-1	−51.7	13.9	−247.0	88.3	9.6	1.5	0.6	147
		876.00	B8-2	−51.8	13.5	−244.5	88.5	9.2	2.2	0.1	885
	Well 9	716.00	B9-1	−52.2	12.7	−247.1	88.1	4.6	7.1	0.2	440
		756.00	B9-2	−51.9	13.7	−245.5	88.9	4.3	6.5	0.3	296
	Well 10	1100.00	B10-1	−45.7	13.6	−243.4	86.8	10.3	1.4	1.5	58
		1160.00	B10-2	−45.8	13.7	−243.5	84.8	12.5	1.6	1.1	77
	Well 11	965.00	B11-1	−56.8	6.7	−248.2	88.1	9	1.6	1.3	68
		1010.00	B11-2	−56.8	6.7	−247.9	87.6	9.5	1.5	1.4	63
JL	Well 1	281.5	J-1	−55.4	−22	−274	26.82	1.95	71.19	0.04	671
	Well 2	325.5	J-2	−58.1	−17.8	−276	31.85	3.31	64.78	0.06	531
	Well 3	332.7	J-3	−56.6	−19.4	−275	35.48	5.86	58.6	0.06	591
	Well 4	336.6	J-4	−59.4	−14.4	−280	49.21	6.65	44.14	0	-
	Well 5	344	J-5	−61.1	−9.8	−281	50.84	5.76	43.33	0.07	726
	Well 6	353.1	J-6	−61.7	−5.8	−280	81.1	0.94	17.93	0.03	2703
	Well 7	364.7	J-7	−58.7	−10.8	−277	91.25	0.82	7.93	0	-
	Well 8	373.2	J-8	−54.8	−19.1	−283	38.9	6.62	54.43	0.05	778
	Well 9	382.6	J-9	−59.7	−9.9	−284	65.52	9.96	24.43	0.09	728
	Well 10	390.8	J-10	−57.9	−14.1	−281	50.51	7.61	41.88	0	-
	Well 11	401.4	J-11	−60.1	−2.7	−283	78.38	9.83	11.72	0.07	1120
	Well 12	415.7	J-12	−58.5	−9.5	−285	60.67	6.97	32.32	0.04	1517
	Well 13	427.3	J-13	−58.1	−10.4	−283	58.68	7.95	33.34	0.03	1956
	Well 14	422.3	J-14	−57.4	−4.9	−284	79.31	9.31	11.33	0.05	1586
	Well 15	469.8	J-15	−50.3	−25.8	−273	30.11	7.94	61.95	0	-
	Well 16	495.8	J-16	−56.7	−11.6	−241	63.56	6.45	29.96	0.03	2119

Note: The symbol "-" represents no relevant data information.

and the JL area (from −25.8‰ to −2.7‰). The $\delta^{13}C(CO_2)$ values in the SR Basin and the MQ area are more narrowly distributed. These characteristics imply that there are multiple sources of CO_2 in mid- to low-rank coal-bearing basins, including pyrolysis, inorganic processes, and microbial action. Therefore, further analysis is required to identify the precise sources of CO_2.

3.3. Coal pyrolysis

Mid- to low-rank coal-bearing basins have undergone varying degrees of coalification. The pyrolysis of coal produces significant quantities of gases, which can significantly affect the proportion of CH_4 and CO_2. To better understand the characteristics of gases generated during the thermal evolution of mid- to low-rank coals, coal samples in the BD (0.62% R_o) and JL (0.35% R_o) areas were obtained for pyrolysis experiments. The results indicate that as the experimental temperature increases, the proportion of CH_4 generation gradually increases, while the proportion of CO_2 generation gradually decreases. A notable difference is observed in the CH_4 and CO_2 generation ratios. For the 0.35% R_o sample, CO_2 generation consistently exceeds that of CH_4 across the temperature range (Fig. 5(a)). Conversely, for the 0.62% R_o sample, CH_4 generation predominates at approximately 500 °C (Fig. 5(b)). The variation in CH_4 and CO_2 generation proportions is more pronounced with increasing temperature in the 0.62% R_o sample.

4. Discussion

4.1. CBM genesis and associated geological process

4.1.1. CBM genesis

Genetic cross plots of gas, initially proposed by Bernard et al. (1976), Schoell (1983), and Whiticar et al. (1986, Whiticar, 1999), have been widely used in the field (Strąpoć et al., 2011; Golding et al., 2013; Vinson et al., 2017; Tang et al., 2022; Zhang et al., 2024). However, these plots were based on relatively small datasets from the 1970s and 1980s, typically involving only tens to several hundred gas samples, which led to less accurate

Table 2
The composition and isotope values in the typical mid- to low-rank coal-bearing basins.

Country	Location	Depth, m	δ^{13}C, ‰		δD, ‰	Gas volume fraction, %				$C_1/(C_2+C_3)$
			CH_4	CO_2		CH_4	CO_2	N_2	C_2+C_3	
China	MQ area	631.27	−52.05	15.86	−239.55	91.98	7.96	0.02	0.04	2295
		515.49	−52.63	10.4	−255.67	94.29	5.53	0.1	0.07	1347
		1165.37	−68.06	−6.8	−274.29	57.87	41.55	0	0.58	100
		532.66	−69.07	−8.05	−257.92	84.57	15.21	0.17	0.02	4229
		793.84	−65.48	−7.03	−257.57	85.02	14.94	0	0.03	2843
		668.23	−68.70	−2.34	−270.65	64.92	34.7	0	0.38	171
		900.36	−67.16	−4.24	−267.44	64.13	35.42	0	0.45	143
		636	−67.89	−2.10	−246.44	79.39	20.28	0.21	0.13	611
		900	−68.91	−3.51	−257.23	54.12	31.55	14.33	0.01	5412
		822	−70.61	−4.41	−262.73	61.78	38.14	0	0.08	772
		625.5	−65.52	−3.71	−224.05	86.78	12.54	0.67	0.01	8678
		890	−68.74	−5.91	−257.21	55.44	44.84	0	0.07	792
		616.59	−77.79	−16.93	−253.45	95.19	4.8	0	0.01	9519
		570.28	−66.31	−4.3	−257.05	97.95	2.02	0	0	9795
		598.42	−63.22	-	−226.37	90.82	0.86	8.31	0.01	9082
	Average		−66.14	−3.08	−253.84	77.62	20.69	1.59	0.13	3719
Australia	SR	284.5	−53.9	-	−227	98.7	0.67	0	0.52	190
	Basin	341	−54.5	-	−235	98.9	0.96	0	0.14	706
		386.2	−52.2	-	−236	94.6	0.6	4.18	0.55	172
		413.2	−51.4	-	−235	98.8	0.75	0	0.41	241
		563.7	−51.2	-	−231	98.6	0.87	0	0.44	224
		586	−50.8	-	−223	99.3	0.59	0.03	0.06	1655
		493	−47.7	-	−224	99.5	0.51	0	0.03	3315
		505.5	−47.8	-	−220	99.3	0.63	0	0.05	1986
		507	−47.5	-	−213	99.4	0.54	0	0.01	9944
		563.8	−45.3	-	−213	99.5	0.44	0	0.03	3318
		589.9	−48	-	−223	99.4	0.62	0	0.03	3312
		620.5	−48.3	-	−226	99.2	0.8	0	0.04	2479
		518	−50.9	-	−213	99.2	0.72	0	0.03	3307
		553.8	−47.4	5.1	−216	99.1	0.83	0	0.05	1982
		596.2	−47.3	4.9	−215	99.3	0.69	0	0.05	1986
		697.2	−50.2	-	−215	97.7	1.12	0	0.54	105
		554.6	−46.8	7.7	−214	99.2	0.71	0	0.05	1984
		522.3	−48.5	-	−224	99	0.49	0.51	0.03	3300
		557.9	−49.2	7.5	−216	99	0.94	0	0.04	2475
		637	−50.1	3.2	−215	98.4	0.77	0	0.66	149
		692.3	−51.1	1.7	−214	98.3	0.69	0	0.85	116
		552.7	−50.3	2.4	−213	99	0.49	0.51	0.04	2478
		491.7	−52.1	6.8	−213	99.2	0.78	0	0.02	4960
	Average		−49.7	4.9	−220	98.8	0.70	0.23	0.20	2190
United States	PR	513.1	−49.2	1.8	-	96.7	0.9	2.40	0	-
	Basin	277	−58.04	11.1	−315.9	88.41	5.3	5.87	0.05	1750
		473	−55.82	11.6	−299.4	84.48	10.69	4.24	0.07	1188
		554	−55.47	10.2	−302.7	81.75	14.06	3.46	0.05	1601
		141	−57.08	12.7	−304	94.64	4.79	0.5	0.07	1352
		481	−56.22	9.1	−292.2	79.17	19.23	1.51	0.09	880
		190	−75.96	−3.4	−321.7	87.93	3.58	7.83	0.12	722
		163	−71.21	−1.2	−319	88.86	4.59	4.73	0.11	768
		144	−69.42	−24.6	−311.9	94.78	3.93	1.16	0.05	1672
		342	−59.24	−13.7	−294	81.42	16.21	2.04	0.15	540
		311	−58.93	14.1	−309.7	89.49	5.17	5.17	0.07	1274
		171	−57.71	10.6	−310.4	70.6	3.95	6.28	-	-
		99	−57.8	10.6	−321.1	73.17	5.73	0.61	0.95	98
		311	−55.52	-	−309.6	88.16	5.95	5.3	-	-
		104	−66.39	8.7	−317.6	93.48	4.93	0.8	0.03	3054
		73	−81.53	10.9	−313.3	88.5	5.21	5.9	0.04	2189
		431	−58.83	−11.1	−290.2	70.06	28.81	0.67	0.15	278
		91	−61.9	−23.5	−309.7	97.95	1.61	0	0.17	572
		227	−60.01	9	−307.4	97.78	1.84	0	0.1	969
		168	−60.71	4.2	−299	97.66	1.66	0.45	0.09	1080
	Average		−62.57	1.67	−307.91	87.25	7.43	2.83	0.13	1203
	SJ	666.4	−46.46	18.16	−208.5	90.78	8.64	0.44	0.14	648
	Basin	701.8	−47.87	16.19	−209.9	95.96	2.61	1.08	0.35	274
		654.7	−47.29	14.37	−216.4	93.17	1.21	1.21	4.41	21
		812.7	−44.62	-	−223.1	87.5	0.07	1.08	11.35	8
		766.6	−44.62	-	−223.3	88	0.16	0.91	10.93	8
		775.4	−42.43	−12.65	−206.8	91.05	0.38	0.24	8.33	11
		872	−42.76	−7.19	−209.3	85.11	0.98	0.23	13.68	6
		723.1	−43.94	−9.58	−212.1	90.06	0.83	0.24	8.87	10
		865.5	−44.46	15.9	−246.9	82.13	17.51	0.07	0.29	283
		888.8	−43.85	14.55	−247.1	84.4	15.06	0.04	0.5	169
		878.9	−43.61	14.63	−241.7	89.22	10.39	0.02	0.37	241
		844.1	−44.11	17.26	−210.1	83.76	15.87	0.02	0.35	239

Table 2 (*continued*)

Country	Location	Depth, m	$\delta^{13}C$, ‰		δD, ‰	Gas volume fraction, %				$C_1/(C_2+C_3)$
			CH_4	CO_2		CH_4	CO_2	N_2	C_2+C_3	
		849.9	−42.98	16.69	−211	85.33	14.34	0.04	0.29	294
		779.7	−44.56	17.01	−209.6	83.78	15.83	0.02	0.37	226
		849.3	−43.85	16.98	−196.6	83.74	15.97	0.01	0.28	299
		808	−44.17	16.9	−199.8	83.14	16.57	0.03	0.26	320
		904	−43.44	16.96	−198.1	83.52	16.01	0.09	0.38	220
		776.5	−44.39	17.12	−201.4	81.37	17.89	0.04	0.7	116
		980.5	−42.8	17.01	−204.2	88.99	10.26	0.36	0.39	228
		920.2	−43.2	16.99	−202.5	87.14	12.54	0.02	0.3	290
		789.4	−43.19	17.21	−199.8	86.6	13.19	0	0.21	412
		899	−43.24	17.03	−200.8	84.04	15.55	0.02	0.39	215
		862.6	−43.32	16.94	−202.8	83.66	16.04	0.02	0.28	299
		919.7	−44.4	16.55	−204.1	87.3	9.59	0.09	3.02	29
		885.9	−44.12	9.4	−203.6	92.51	1.96	0.09	5.44	17
		909.8	−43.81	17.03	−204.3	81.47	18.01	0.02	0.5	163
	Average		−44.13	13.0	−211.3	86.7	10.3	0.25	2.78	194

Note: The relevant composition and isotopic data of CBM were collected from Zhou et al. (2005), Flores et al. (2008), Hamilton et al. (2014), and Li et al. (2021a); The symbol "-" represents no relevant data information.

identification of gas genesis. Milkov and Etiope (2018) modified these plots by incorporating a more extensive geochemical and geological dataset from various regions.

The genetic cross plots of $C_1/(C_2+C_3)$ versus $\delta^{13}C(CH_4)$ (Fig. 6(a)) and $\delta^{13}C(CO_2)$ versus $\delta^{13}C(CH_4)$ (Fig. 6(c)) indicate that most gas samples from the MQ area are predominantly associated with primary microbial gas, primarily generated through CO_2 reduction. Additionally, some gas samples from the MQ area are found in the early mature thermogenic gas field. The plots in Fig. 6(a) and (c) reveal that the majority of gas samples from the JL area fall within the overlapping or transitional field between early mature thermogenic gas and primary or secondary microbial gas (generated by CO_2 reduction and methyl-type fermentation pathways). This phenomenon also suggests that distinguishing the boundary between early mature thermogenic and microbial gases is difficult. This difficulty arises because gas generation likely represents a transitional process rather than a distinct shift from purely microbial to thermogenic processes (Scott et al., 1994; Flores et al., 2008; Strąpoć et al., 2011; Moore et al., 2014; Milkov and Etiope, 2018; Tang et al., 2022).

Fig. 6(a) and (c) demonstrate that gas samples from the SJ Basin are located in the overlapping or transitional field between middle mature thermogenic gas and secondary biogenic gas. Additionally, the CO_2 carbon isotope ranges in the SJ Basin include low negative to positive carbon isotope values suggesting that secondary biogenic processes and CO_2 reduction pathway are widespread (Fig. 6(e)). The abundant $^{13}CO_2$ can be explained as the continuous enrichment of $^{13}CO_2$ in the substrate due to preferentially using ^{12}C during the microbial process of CO_2 reduction to produce CH_4 ($CO_2 + 4H_2 \rightarrow CH_4 + 2H_2O$) (Clayton, 1998; Whiticar, 1999; Wang et al., 2022; Tang et al., 2022). The BD area and SR Basin also show similar characteristics, which indicates that these two areas also generated thermogenic gas and underwent biodegradation. Gas samples from the PR Basin show similar characteristics to those of the JL area (Fig. 6(a) and (c)). The negative to positive carbon isotope of CO_2 in PR Basin implies that the basin has undergone significant secondary biogenic processes (Fig. 6(e)).

4.1.2. CO_2 genesis

As mentioned above, there are substantial differences in the CO_2 volume fraction of coal across different basins. Specifically, the CO_2 volume fraction increases with burial depth in the PR Basin, JL area, BD area, and MQ area (Fig. 3). The origin of CO_2 among different coal-bearing basins is preliminarily analyzed by $\delta^{13}C(CO_2)$ versus CDMI (Fig. 7). As shown in Fig. 7, all gas samples from the SR Basin, along with most samples from the SJ Basin, PR Basin, MQ area, and

Table 3
Comparative analysis of relevant data of typical mid- to low-rank coal-bearing basins.

Country	Basin/ area	Properties								
		Burial depth, m	R_o, %	TDS, mg/L	CH_4 volume fraction, %	CO_2 volume fraction, %	$\delta^{13}C(CH_4)$, ‰	$\delta D(CH_4)$, ‰	$\delta^{13}C(CO_2)$, ‰	CBM genesis (main)
China	MQ	0–1500	<0.5	1938 –44490	54.12–97.95	0.86–44.84	−52.05 to −77.79	−226.37 to −274.29	−16.93 to 15.86	Primary biogenic
	BD	0–1200	0.52 –0.89	1403 –14886	84.4–93.1	1.8–12.5	−45.7 to −61.8	−242.4 to −259.4	−10.5 to 13.9	Secondary biogenic and thermogenic gas
	JL	0–1000	0.28 –0.6	1604 –6400	26.82–91.25	0.82–9.96	−50.3 to −61.7	−241 to −285	−25.8 to −2.7	Secondary biogenic gas
United States	PR	0–900	0.31 –0.49	370 –1940	70.06–97.95	0.9–28.81	−49.2 to −81.53	−321.7 to 290.2	−24.6 to 14.1	Secondary biogenic gas
	SJ	0–1600	0.7–1.5	<42000	81.37–93.17	0.07–18.01	−42.43 to −47.87	−196.6 to −247.1	−12.65 to 18.16	Secondary biogenic and thermogenic gas
Australia	SR	0–850	0.35 –0.7	792 –10177	94.6–99.5	0.44–1.12	−45.3 to −54.5	−213 to −236	1.7 to 7.7	Secondary biogenic gas

The relevant data of the China from Sun et al. (2018), Tao et al. (2019c), Fu et al. (2021), Li et al. (2021a), the United States from Ayers (2002), Zhou et al. (2005), Flores et al. (2008), and the Australia from Hamilton et al. (2014), Tang et al. (2018). TDS: total dissolved solids.

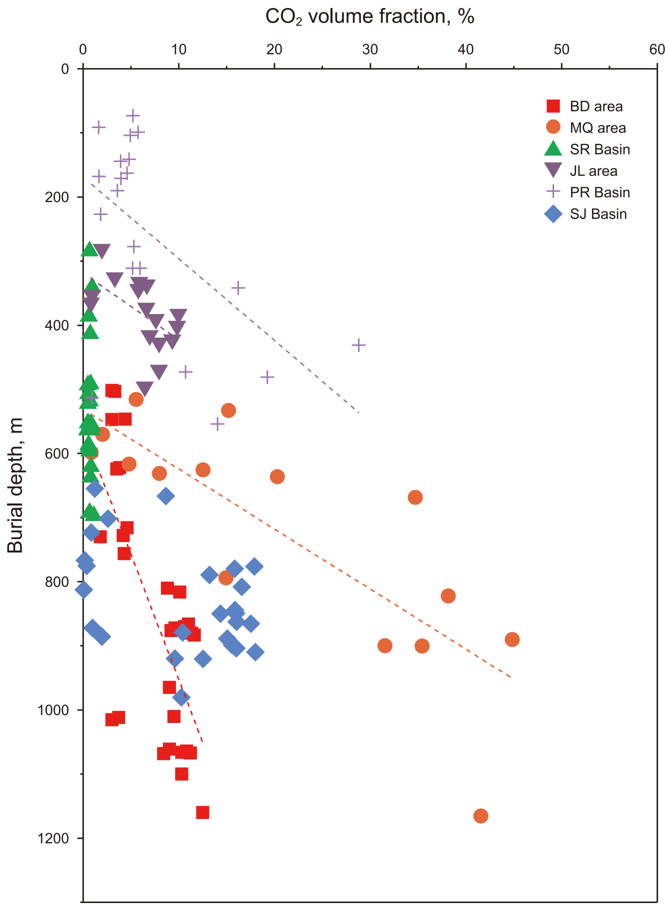

Fig. 3. CO_2 volume fraction versus burial depth of coals in different areas or basins.

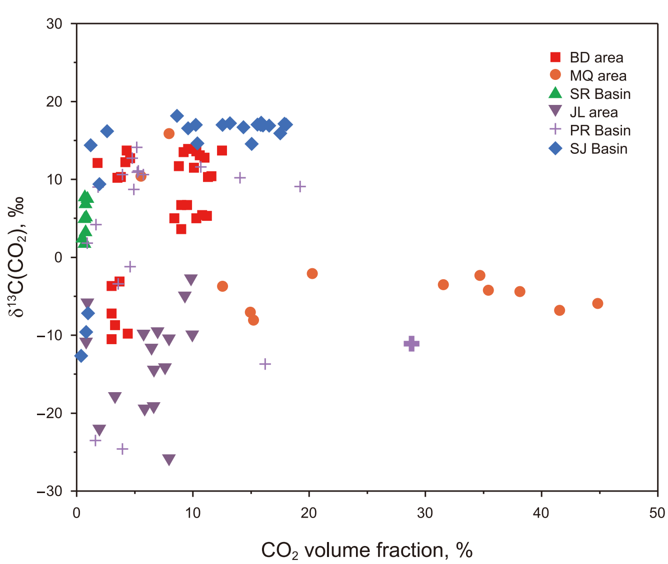

Fig. 4. $\delta^{13}C(CO_2)$ versus CO_2 volume fraction in different areas or basins, showing a wide range of values.

BD area, fall within the field associated with microbial methanogenesis. According to the analysis of CBM genesis, CO_2 in the SJ Basin and BD area primarily originates from thermogenic processes and microbial degradation. Methanogens exert a significant fractionation effect on carbon isotopes, preferentially utilizing lighter ^{12}C and generating $^{12}CO_2$ during coalification (Vinson et al., 2017). Consequently, biogenic CH_4 has lighter carbon isotopes, whereas the CO_2 in the substrate becomes heavier. In the MQ area, PR Basin, and SR Basin, the CO_2 is mainly related to microbial methanogenesis, with some contribution from thermogenic processes. It is worth noting that the $\delta^{13}C(CO_2)$ values in the JL area are obviously negative, and most gas samples are located in the field associated with thermogenic methanogenesis (Fig. 7). However, the CBM genesis analysis suggests that the JL area shows biogenic gas characteristics rather than thermogenic. Moreover, the lower degree of coalification (0.28%–0.6% R_o) in the JL area may not have experienced substantial thermogenic gas generation. Therefore, the CO_2 in the JL area is mainly derived from microbial degradation process, with some contribution from thermogenic processes.

4.1.3. *Associated geological process*

Coal possesses a higher total organic carbon content compared to other source rocks and produces a greater quantity of low molecular weight organic intermediate compounds during biodegradation (Gao et al., 2013; Vinson et al., 2017). The bacteria convert the geopolymer in source rock organic matter into these low molecular weight organic intermediates (Fig. 8), which are subsequently transformed into methane precursors, such as acetate, H_2, formate, and CO, etc (Flores et al., 2008; Strąpoć et al., 2011; Vinson et al., 2017). Finally, the methanogens convert methane precursors into methane, which is the final step of biodegradation (Fig. 8). The CO_2 is a byproduct of this entire biodegradation sequence. Various pathways guide carbon conversion throughout this sequence (Fig. 8). There are two main pathways for methanogens: (1) the reduction of methyl groups to methane and the oxidation of carboxyl groups to CO_2, known as acetate fermentation or acetotrophic methanogenesis, and (2) the reduction of CO_2 to methane using H_2, referred to as CO_2 reduction or hydrogenotrophic methanogenesis (Whiticar et al., 1986; Whiticar, 1999; Strąpoć et al., 2011; Golding et al., 2013; Vinson et al., 2017). Beyond the widely recognized acetotrophic methanogenesis and hydrogenotrophic methanogenesis, there are also the methylotrophic methanogenesis process (Golding et al., 2013; Vinson et al., 2017). However, the methylotrophic methanogenesis pathway is considered unimportant compared to the hydrogenotrophic methanogenesis pathways and acetotrophic methanogenesis pathways on a global scale (Vinson et al., 2017).

In the early stages of coalification in the peat swamp, methanogens can produce significant amounts of primary microbial gas at relatively low temperatures and burial depths (R_o < 0.3%) (Scott et al., 1994; Golding et al., 2013; Vinson et al., 2017; Tang et al., 2022). However, the primary microbial gas has always been controversial. Some studies suggest that primary microbial gas can be retained (in a sorbed or free state) by coal or dissolved in pore water (Scott et al., 1994). However, despite the large pore space of peat, the higher moisture content of peat occupies potential adsorption sites for primary microbial gas. As a result, primary microbial gas is usually not retained in significant quantities, and most of the gas is removed during later compaction and coalification (Scott et al., 1994). For example, the PR Basin and JL area only partial primary microbial gas characteristics (Fig. 6). However, under some special hydrogeological conditions, primary biogas can be retained by coal, for example, the MQ area exhibits significant primary microbial gas characteristics (Fig. 6). The high total dissolved solids (TDS) in the coal seam water of the MQ area indicate a stagnant groundwater environment. Additionally, coal seam water dating experiments suggest that the age of coal seam water in the MQ area is ancient, with coal seam water and CBM having similar geological ages (Fu et al., 2019, 2021; Tang et al., 2022). This minimal structural damage from atmospheric/surface water allows the

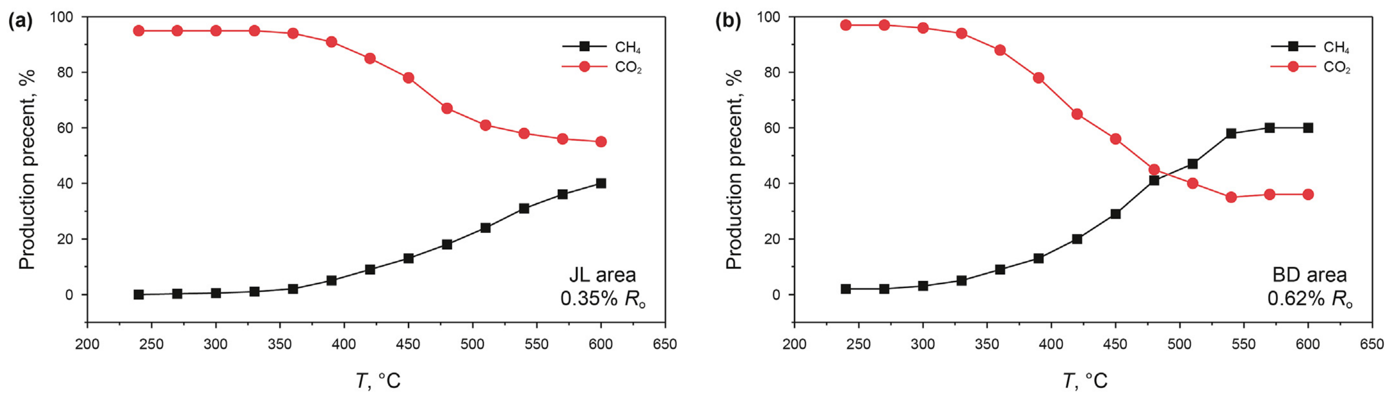

Fig. 5. CH_4 and CO_2 generation proportion during coal pyrolysis. The coal samples from the JL area and BD area were collected (0.35% R_o and 0.62% R_o, respectively).

preservation of primary microbial gas in the MQ area. In fact, most biogenic gases in coals are associated with groundwater and generated through secondary microbial processes. Unlike primary microbial gas, secondary biogenic gas is produced when methanogens are introduced into coals after burial, coalification, and uplift of basin margins (Scott et al., 1994; Golding et al., 2013; Vinson et al., 2017). Methanogens metabolize wet gas components, n-alkanes, and other organic compounds to generate substantial quantities of secondary biogenic gas (Fig. 8). For example, the SR Basin, PR Basin, SJ Basin, BD area, and JL area all show obvious characteristics of secondary biogenic gas (Fig. 6).

In addition to microbial processes, thermogenic methane generation pathways also exist in mid- to low-rank coal-bearing basins (Strąpoć et al., 2011; Tang et al., 2022; Wang et al., 2022). The generation of thermogenic CBM is divided into early stage and main stage. Early thermogenic gas is mainly generated by high volatile bituminous coals (0.5%–0.8% R_o), which is the main source of thermogenic gas in mid- to low-rank coal-bearing basins (Scott et al., 1994). Examples include the SR Basin, MQ area, BD area, and JL area. Early thermogenic gases typically include CH_4, CO_2, and some wet gas components, but there are variations in the proportions of CH_4 generation. The transformation ratio (TR) refers to the degree of conversion of organic matter to hydrocarbons during thermal maturation process, ranging from 0 (no conversion) to 1 (complete conversion). Previous research has shown that the TR values for coal can reach 0.1 at 0.7% R_o, with hydrocarbon gas generation increasing rapidly from 0.7% to 1.6% R_o, and TR values reaching up to 0.8 (Waples and Marzi, 1998). The remaining 20% of hydrocarbon gas generation continues until the anthracite maturity range (2.5%–5% R_o) (Schimmelmann et al., 2006). These studies indicate that the proportion of `hydrocarbons in early thermogenic CBM is very low. To further understand the proportion of CH_4 generation during early thermal maturation process, coal samples from the JL and BD areas (0.35% R_o and 0.62% R_o, respectively) were collected for thermal simulation experiments (Fig. 5). This experiment confirms that the proportion of CH_4 generation during early thermal maturation process is significantly lower than that of CO_2. Therefore, the contribution of early thermal maturation processes to CH_4 in mid- to low-rank coal-bearing basins is likely limited, while microbial processes are critical for CH_4 generation.

In the biodegradation sequence, the generation of CH_4 is the final step in the biodegradation of organic carbon, and it significantly affects the isotopic fractionation of carbon atoms (Fig. 8) (Strąpoć et al., 2011; Vinson et al., 2017). The ^{12}C-rich substrates can be more effectively utilized compared to ^{13}C-rich substrates. As a result, the CO_2 reduction pathway produces lighter CH_4 carbon isotopes and heavier residual CO_2 carbon isotopes. In acetate fermentation, the methyl carbon of acetate has less ^{13}C, while the carboxyl carbon has more ^{13}C (Vinson et al., 2017). This results in CH_4 with lighter carbon isotopes, while the accompanying CO_2 may have heavier carbon isotopes ($CH_3COOH \rightarrow CH_4 + CO_2$). Thermogenic processes also affect carbon isotope fractionation. The bond energy of $^{13}C-^{13}C$ is the highest, followed by $^{12}C-^{13}C$ and $^{12}C-^{12}C$. As a result, early thermal maturation processes tend to produce more negative $\delta^{13}C(CH_4)$ and $\delta^{13}C(CO_2)$ values, leading to the overlapping fields of early thermogenic gas with the biogenic gas (Figs. 6 and 8). As thermal maturity increases, the $\delta^{13}C(CH_4)$ values become more positive with increasing coal rank (Strąpoć et al., 2011; Golding et al., 2013; Vinson et al., 2017). However, the range of such positive values may be limited in mid- to low-rank coal-bearing basins. On the one hand, the lower thermal evolution temperature restricts the positive values of $\delta^{13}C(CH_4)$. On the other hand, secondary microbial processes in the basin can modify the signature of $\delta^{13}C(CH_4)$ values (Scott et al., 1994). For example, despite large differences in coal rank (from 0.7% to 1.5% R_o) in the northern part of the SJ Basin, $\delta^{13}C(CH_4)$ values in coals remain consistent due to secondary microbial processes (Fig. 6; Scott et al., 1994).

4.2. Migration and accumulation model of CBM

The genesis of CBM in the mid- to low-rank coals is complex, and a single geochemical data cannot completely analyze the genesis and source of the gas. Correlating microbial processes, coal thermal evolution processes, hydrogeological conditions, basin tectonic morphology, and geochemical data can provide more valuable information on CBM genesis, migration, and accumulation.

4.2.1. Hydrodynamic active monoclinic model

The BD area is characterised by a west-dipping monoclinal tectonics with a small dip angle (Fig. 9). The Ro in this area ranges from 0.52% to 0.89%, and the burial depth can reach up to 1200 m (Tian et al., 2012; Li et al., 2021b). The deeper coals show the characteristics of thermogenic gas. Due to tectonic movements, the northern part of the basin gradually uplifted towards the surface, causing the continuous escape of thermogenic gas. At the same time, under the action of surface water, the coals underwent microbial reinoculation (Fig. 9). Methanogens then metabolized wet gas components, *n*-alkanes, and other organic compounds, producing large quantities of secondary biogenic gas. Additionally, the volume fraction of CO_2 in the BD area shows an increasing trend with increasing burial depth (Fig. 3). This is because methanogens proliferate in the shallow coals, leading to significant CO_2 consumption. However, as burial depth increases, high temperature,

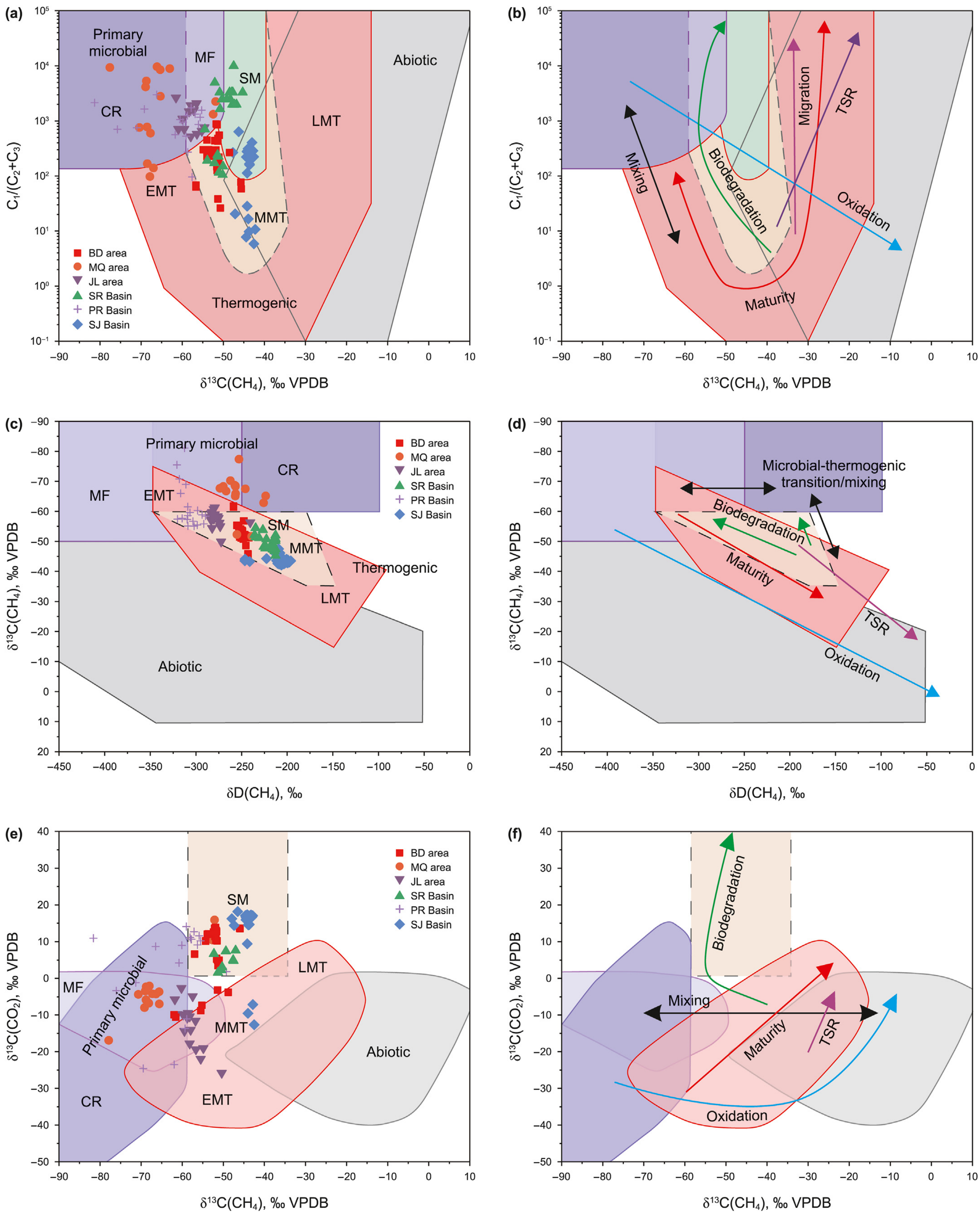

Fig. 6. Genetic cross plot of CBM from typical mid- to low-rank coal-bearing basins at home and abroad (modified after Milkov and Etiope (2018)). (**b**), (**d**), and (**f**) provide explanations for factors influencing the composition and isotopic variation of the gases shown in (**a**), (**c**), and (**e**), respectively. The abbreviations used are as follows: CR for CO_2 reduction, MF for methyl-type fermentation, SM for secondary microbial, EMT for early mature thermogenic gas, MMT for middle mature thermogenic gas, LMT for late mature thermogenic gas, and TSR for thermochemical sulphate reduction.

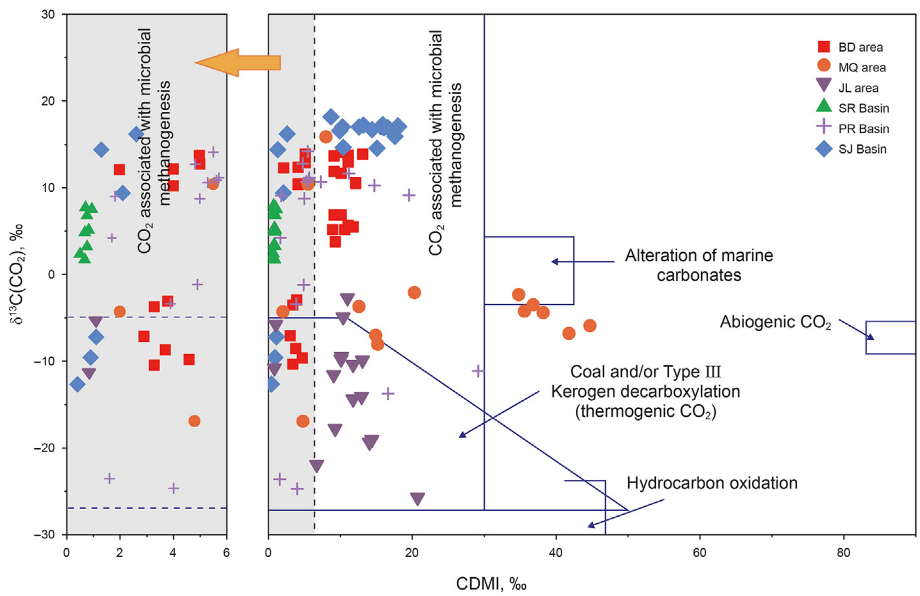

Fig. 7. The cross plot of $\delta^{13}C(CO_2)$ versus CDMI showing the genesis of CO_2 (modified after Kotarba (2001)).

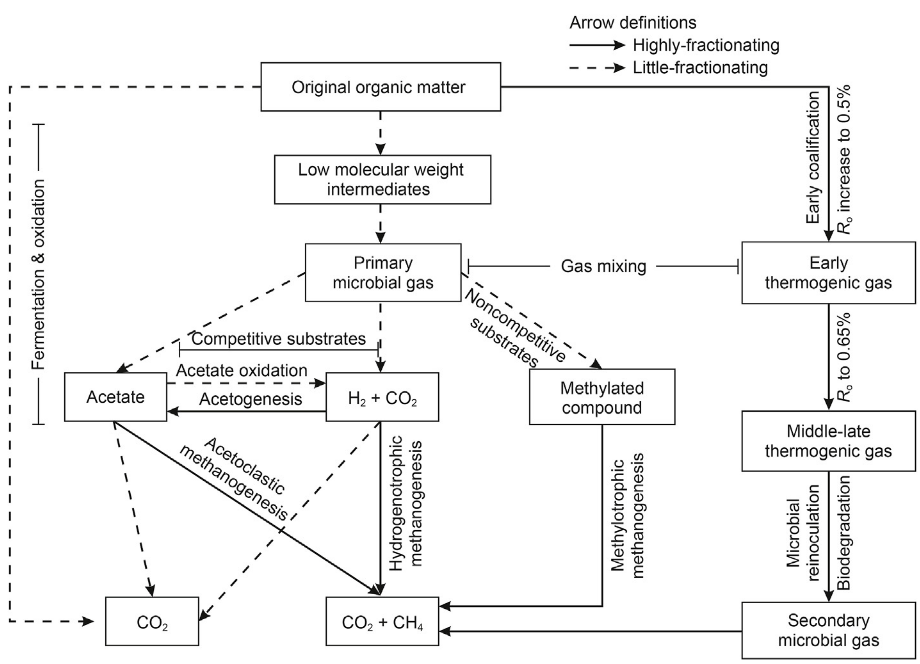

Fig. 8. Schematic diagram showing methanogenesis biodegradation pathways (modified from Whiticar, 1999; Flores et al., 2008; Vinson et al., 2017).

high pressure, and high TDS inhibit methanogen activity, resulting in slower CO_2 consumption in deeper coals compared to shallower ones. Moreover, CO_2 easily dissolves in groundwater and migrates with it to deeper coals. The BD area also features nose-like structures, where gas migrates and accumulates at the top of these structures due to hydrodynamic forces.

In addition to the BD area, the SR, and PR Basins also show similar tectonic morphologies (Figs. 10 and 11; Flores et al., 2008; Baublys et al., 2015; Tang et al., 2018). Compared to the thicker coals in the BD area, the coals in the SR Basin show more layers and less thickness, with burial depth of up to 800 m (Hamilton et al., 2012, 2014). The SR Basin features westward-dipping monoclinal tectonics and regionally developed nose-like structures (Fig. 10; Hamilton et al., 2012, 2014). The coals exposed in the eastern part of the basin have undergone recharge by flowing water and microbial reinoculation, resulting in the generation of significant amounts of secondary biogenic gas (Fig. 10). Some early thermogenic gas (0.35%–0.7% R_o) is present in the deeper parts of the SR Basin. The gas is enriched at the high points of the nose-like structures under hydrodynamic lateral sealing (Hamilton et al., 2014; Tang et al., 2018). In contrast, the coals in the PR Basin have a low R_o (<0.5%) with a burial depth of up to 800 m (Flores et al., 2008). Consequently, the PR Basin has not experienced significant thermogenic gas generation. Groundwater is more active in the PR Basin than in the BD area and SR Basin, with TDS ranging from 370 to 1940 mg/L (Table 3; Ayers, 2002). The coals exposed in the eastern part of the

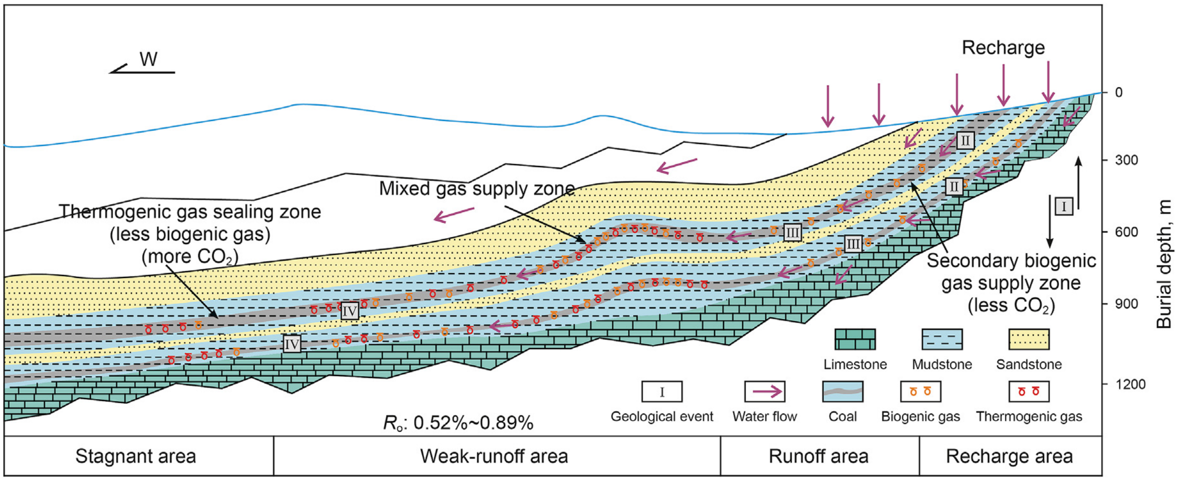

Fig. 9. The formation of secondary biogenic gas and thermogenic gas within the hydrodynamic active area in the BD area. I: Burial and coalification are followed by basin uplift and erosion along basin margin; II: Meteoric water transports methanogens basinward from recharge area; III: Methanogens metabolize wet gas components, *n*-alkanes, and other organic compounds in the coal to generate secondary biogenic gas; IV: Hydrodynamic trapping of thermogenic gas and secondary biogenic gas.

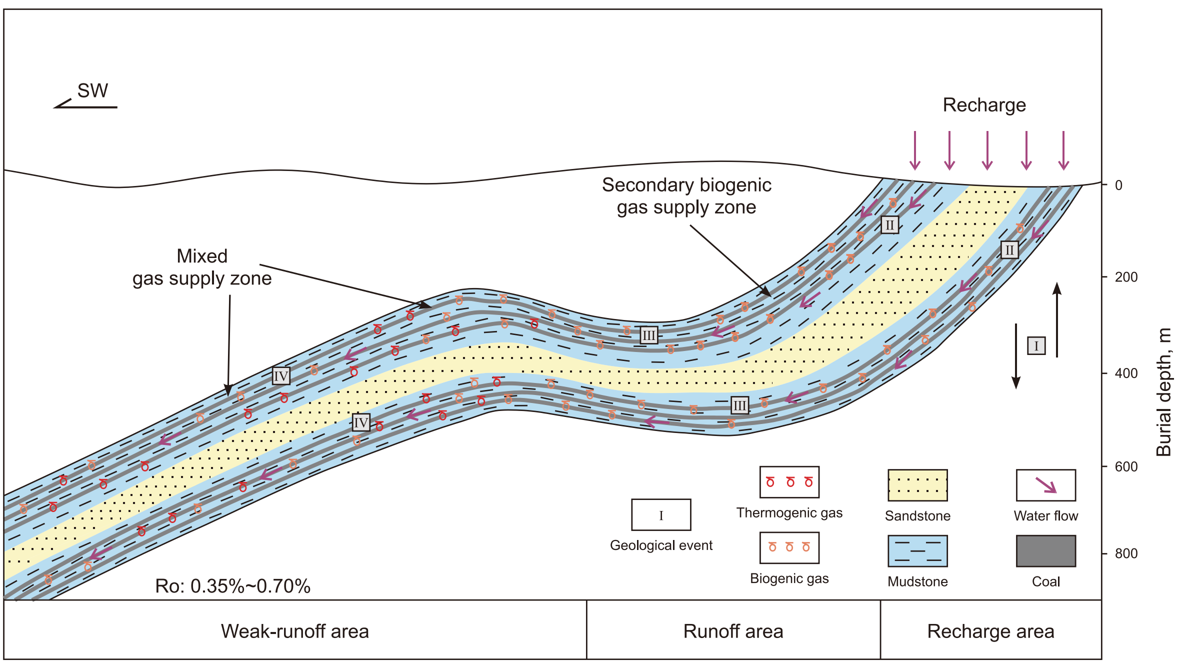

Fig. 10. The formation of the secondary biogenic gas and less thermogenic gas within the hydrodynamic active area in the SR Basin (modified from Tang et al. (2018)). I: Burial and coalification are followed by basin uplift and erosion along basin margin; II: Meteoric water transports methanogens basinward from recharge area; III: Methanogens metabolize wet gas components, *n*-alkanes, and other organic compounds in the coal to generate secondary biogenic gas; IV: Minor migrated thermogenic gas and secondary biogenic are mixed.

Basin have experienced microbial reinoculation and have produced significant amounts of secondary biogenic gas (Flores et al., 2008). Unlike the nose-like structures in the BD area and SR Basin, the PR Basin shows microstructural characteristics. Here, the coals are usually pinch-outed or blocked by sandstones, with gas enrichment primarily occurring in these secondary folds and pinch-out areas due to hydrodynamic forces (Fig. 10; Ayers, 2002; Flores et al., 2008).

Therefore, in view of the above characteristics, one of the migration-accumulation models of CBM in mid- to low-rank coal-bearing basins can be summarized as a hydrodynamic active monoclinic model. In this model, hydrodynamics plays a is usually more active, with methanogens transported by flowing water generating substantial amounts of secondary biogenic gas in the shallow sections, while thermogenic gas is present in deeper sections (depending on the thermal evolution degree of the coals). CBM enrichment predominantly occurs at tectonic highs or other specific tectonic locations.

4.2.2. Hydrodynamic differential syncline model

The JL area is characterized by isolated secondary fault depressions, which can also be regarded as a gently syncline structure (Fig. 12; Guo et al., 2022). The coals in this area exhibits a gentle dip with a burial depth of up to 600 m and R_o ranging from 0.28% to 0.6% (Fig. 12; Tao et al., 2019c). Shallow burial depths and low TDS (from 1604 to 6400 mg/L) provide favorable conditions for

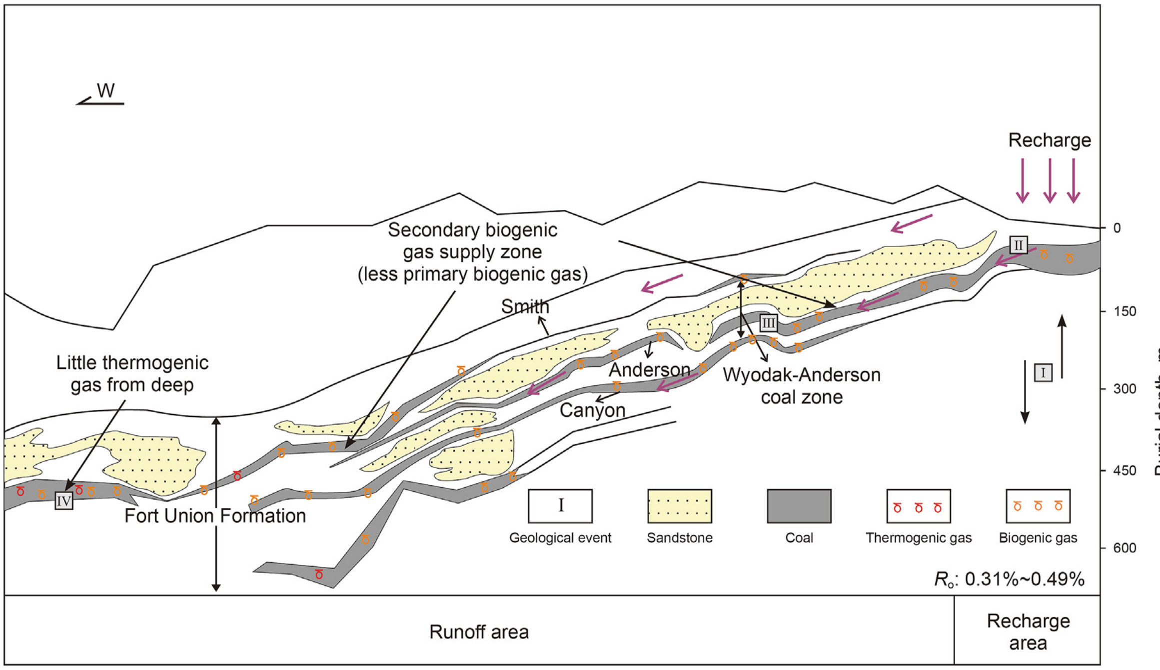

Fig. 11. The formation of the secondary biogenic gas within the runoff area in the PR Basin (modified from Flores et al. (2008)). I: Burial and coalification are followed by basin uplift and erosion along basin margin; II: Meteoric water transports bacteria basinward from recharge area; III: Methanogens metabolize organic compounds into secondary biogenic gas; IV: Secondary biogenic gas is sealed by structural trap and physical property change, and a small amount of thermogenic gas migrated upward from deep.

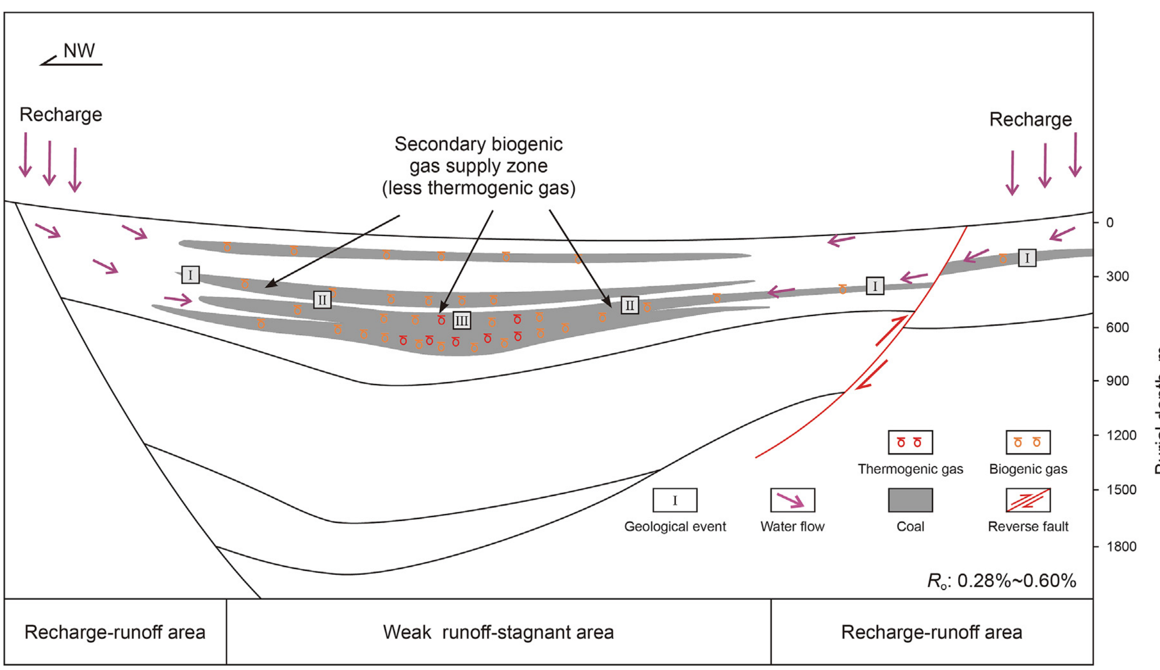

Fig. 12. The formation of the secondary biogenic gas and little thermogenic gas in the JL area (modified from Sun et al. (2018)). I: Meteoric water transports methanogens basinward from recharge area; II: Methanogens metabolize organic compounds into secondary biogenic gas; III: Hydrodynamic trapping of secondary biogenic gas and little thermogenic gas.

methanogens activity. The northwestern and southeastern branches of the syncline were recharged by atmospheric precipitation, leading to microbial reinoculation of the coals. Methanogens metabolize organic compounds to produce large amounts of secondary biogenic gas. Additionally, the volume fraction of CO_2 in JL area increases with burial depth (Fig. 3). In the tectonic morphology of syncline, groundwater alternately stagnates near the core of the syncline, which tends to form higher pressure and higher TDS, which is unfavorable for microbial gas generation, but a small amount of thermogenic gas may exist (Fig. 12). The gas is enriched in the core of the syncline by the hydrodynamic sealing effect on both sides of the syncline (Fig. 12).

Large-dip structures are developed in the syncline of the MQ area (Fig. 13). The northern and southern parts of the syncline are

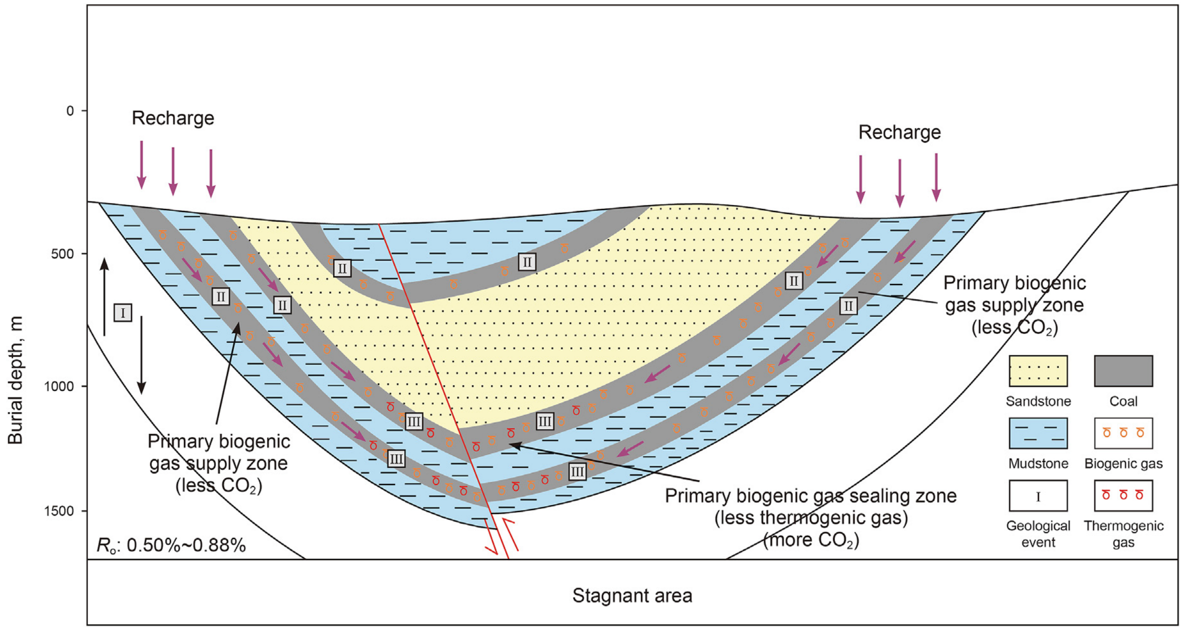

Fig. 13. The formation of primary biogenic gas within the stagnant area of the MQ area (modified from Li et al. (2021a)). I: Basin uplift and erosion in the MQ area; II: Meteoric water transports methanogens basinward from recharge area, and methanogens metabolize coal organic matter to generate primary biogenic gas; III: Hydrodynamic trapping of primary biogenic gas and minor amounts of thermogenic gas.

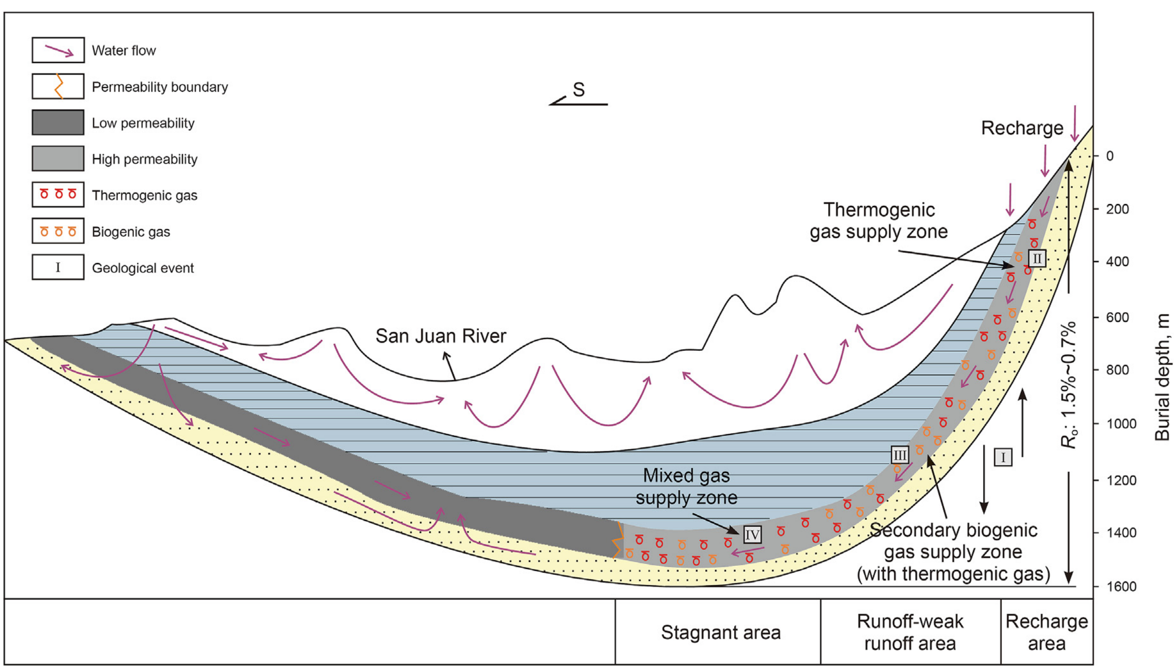

Fig. 14. The formation of secondary biogenic gas and thermogenic gas in the SJ Basin (modified from Scott et al. (1994) and Ayers (2002)). I: Burial and coalification are followed by basin uplift and erosion along basin margin; II: Meteoric water transports methanogens basinward from recharge area; III: Methanogens metabolize wet gas components and n-alkanes to generate secondary biogenic gas; IV: Thermogenic gas and secondary biogenic gas are sealed by artesian overpressure and physical property change.

recharged by atmospheric precipitation. The coals in this area have a R_o ranging from 0.5% to 0.88% and reach burial depths of up to 1500 m (Li et al., 2021a). Due to the tectonic conditions of large dips, groundwater tends to stagnate in the synclinal core, making the MQ area a catchment center with TDS reaching up to 44,490 mg/L (Fu et al., 2021). The CBM in the MQ area exhibits characteristics typical of primary biogenic gas (Fig. 6). Fu et al. (2021) indicated that the geological age of the coal seam water in the MQ area is relatively old, with little to no influx of modern water. The high TDS environment further suggests that the current coal seam water is not conducive to the survival of methanogens or the generation of CH_4. Therefore, the MQ area is classified as an old, closed primary biogenic gas reservoir (Fig. 13). Additionally, the volume fraction of CO_2 in coal seams of the MQ area show an increasing trend with burial depth, reaching up to 44.84% (Fig. 3). This is attributed to the high pressure and high TDS in the deeper layers, which inactivate methanogens and halt CO_2 consumption. The CO_2 in the shallow layers dissolves in water and migrates with groundwater to the deeper layers within the MQ area (Fu et al., 2021).

Therefore, based on the above characteristics, another model of CBM migration-accumulation in mid- to low-rank coal-bearing basins can be summarized as the hydrodynamic differential syncline model. In this model, differential hydrodynamic characteristics are more pronounced, with shallowly generated gas typically migrating towards the syncline core due to hydrodynamic forces.

Furthermore, the SJ Basin demonstrates a combination of the two previously discussed models. The northern part of the SJ Basin is characterized by a monoclinal structure, while the central region forms a synclinal structure (Fig. 14). The high-temperature heat flow from volcanic activity in the north has resulted in significant variations in the thermal maturity of coals, with Ro values decreasing from 1.5% in the northern part of the basin to 0.7% in the center (Scott et al., 1994; Ayers, 2002). Consequently, the northern coals generate a substantial amount of thermogenic gas (Fig. 14). Additionally, exposed coals in the northern region have been recharged by atmospheric precipitation and subsequently underwent microbial reinoculation (Ayers, 2002; Zhou et al., 2005). Methanogens metabolize wet gas components, n-alkanes, and other organic compounds to produce large quantities of secondary biogenic gas. Both shallow thermogenic gas and secondary biogenic gas are trapped in the core of the syncline by hydrodynamic forces (Fig. 14).

Overall, the flow of groundwater plays a critical role in the generation and migration of gas within mid- to low-rank coal-bearing basins (Scott et al., 1994; Ayers, 2002; Strąpoć et al., 2011; Golding et al., 2013; Vinson et al., 2017). Primary biogenic gases generated during early stages are typically not adsorbed or preserved by coal, with most gases found in coals being secondary biogenic gases resulting from bacterial inoculation (Scott et al., 1994). These basins generally experience a history of burial, coalification, and subsequent uplift and erosion along basin margins (Scott et al., 1994; Vinson et al., 2017; Fu et al., 2021). Methanogens, introduced into coals through atmospheric precipitation and groundwater, generate significant quantities of secondary biogenic gas. Consequently, the presence of biogenic gas in these basins is primarily controlled by their hydrogeological conditions. Additionally, the enrichment of CBM in mid- to low-rank coal-bearing basins is influenced by basin or regional tectonic structures. As discussed, gas enrichment is more likely to occur in tectonic highs, syncline centers, secondary folds, and pinch-out areas under hydrodynamic control. Based on the above discussion, the genesis, migration, and accumulation models of CBM in mid- to low-rank coal-bearing basins can be categorized into two models—the hydrodynamic active monoclinic model and the hydrodynamic differential syncline model—or a combination of the two.

5. Conclusions

Based on systematic analyses of the BD and JL areas, this paper compares the genesis, associated geological processes, and migration-accumulation models of CBM in several typical mid- to low-rank coal-bearing basins. The following conclusions can be drawn.

(1) Biogenic gases are extensively developed in mid- to low-rank coal-bearing basins. In the BD area and the SJ Basin, CBM is predominantly thermogenic and secondary biogenic. The CBM in the MQ area is characterized by primary biogenic gas. In contrast, the SR Basin, PR Basin, and JL area are characterized by secondary biogenic gas. Microbial CO_2 reduction occurs in mid- to low-rank coal-bearing basins, significant gas production from acetate fermentation is observed in certain regions.

(2) The genesis of CO_2 is related to early coalification and microbial process. In the PR Basin, SR Basin, and JL area, CO_2 was produced through the microbial degradation of organic matter. The volume fraction of CO_2 increases with burial depth, influenced by selective microbial metabolism and differential dissolution in groundwater (e.g., MQ area, BD area, JL area, and PR Basin). In other basins studied, CO_2 initially originates from coal pyrolysis and is subsequently supplemented by CO_2 generated through microbial methanogenesis.

(3) The flow of groundwater is crucial for the generation and migration of gas in the mid- to low-rank coal-bearing basins. Based on the analysis of microbial processes, coal thermal evolution processes, hydrogeological conditions, basin tectonic morphology, and geochemical data, the migration-accumulation models of CBM in mid- to low-rank coal-bearing basins can be categorized into two models—the hydrodynamic active monoclinic model and the hydrodynamic differential syncline model—or a combination of the two.

CRediT authorship contribution statement

Bin Zhang: Writing – original draft, Methodology, Data curation. **Shu Tao:** Supervision, Project administration. **Fan Yang:** Supervision, Project administration. **Yi Cui:** Supervision. **Qing-He Jing:** Supervision. **Jie Guo:** Supervision. **Shi-Da Chen:** Supervision, Data curation. **Yi-Jie Wen:** Data curation. **Xin-Yang Men:** Data curation.

Declaration of competing interest

The authors declare that they have no known competing financial interests or personal relationships that could have appeared to influence the work reported in this paper.

Acknowledgments

This work was financially supported by the National Natural Science Foundation of China (No. 42272200), The Science and Technology Major Project of China National Petroleum Corporation (No. 2023ZZ18-03), The Science and Technology Major Project of Changqing Oilfield (No. 2023DZZ01). The Technology project of Huaneng Group Headquarters (Medium-deep Low-Rank Coalbed Methane Resource Potential Evaluation and Key Development Technologies of Zhalainuoer Coalfield, No. HNKJ23-H51). The authors also thank the reviewers and editors for their constructive comments and suggestions on improving this manuscript.

References

Ayers, W.B., 2002. Coalbed gas systems, resources, and production and a review of contrasting cases from the San Juan and Powder River basins. AAPG (Am. Assoc. Pet. Geol.) Bull. 86 (11), 1853–1890. https://doi.org/10.1306/61EEDDAA-173E-11D7-8645000102C1865D.

Bernard, B.B., Brooks, J.M., Sackett, W.M., 1976. Natural gas seepage in the gulf of Mexico. Earth Planet Sci. Lett. 31 (1), 48–54. https://doi.org/10.1016/0012-821X(76)90095-9.

Bates, B.L., McIntosh, J.C., Lohse, K.A., Brooks, P.D., 2011. Influence of groundwater flowpaths, residence times and nutrients on the extent of microbial methanogenesis in coal beds: Powder River Basin, USA. Chem. Geol. 284 (1–2), 45–61. https://doi.org/10.1016/j.chemgeo.2011.02.004.

Baublys, K.A., Hamilton, S.K., Golding, S.D., Vink, S., Esterle, J., 2015. Microbial controls on the origin and evolution of coal seam gases and production waters of the Walloon Subgroup; Surat Basin, Australia. Int. J. Coal Geol. 147–148, 85–104. https://doi.org/10.1016/j.coal.2015.06.007.

Boreham, C.J., Edwards, D.S., 2008. Abundance and carbon isotopic composition of neo-pentane in Australian natural gases. Org. Geochem. 39 (5), 550–566. https://doi.org/10.1016/j.orggeochem.2007.11.004.

Clayton, J.L., 1998. Geochemistry of coalbed gas - a review. Int. J. Coal Geol. 35 (1–4), 159–173. https://doi.org/10.1016/S0166-5162(97)00017-7.

Chen, Y., Tang, D.Z., Xu, H., Li, Y., Meng, Y.J., 2015. Structural controls on coalbed methane accumulation and high production models in the eastern margin of Ordos Basin, China. J. Nat. Gas Sci. Eng. 23, 524–537. https://doi.org/10.1016/j.jngse.2015.02.018.

Dai, J.X., Xia, X.Y., Li, Z.S., Coleman, D.D., Dias, R.F., Gao, L., Li, J., Deev, A., Li, J., Dessort, D., Duclerc, D., Li, L.W., Liu, J.Z., Schloemer, S., Zhang, W.L., Ni, Y.Y., Hu, G.Y., Wang, X.B., Tang, Y.C., 2012. Inter-laboratory calibration of natural gas round robins for δ^2H and δ^{13}C using off-line and on-line techniques. Chem. Geol. 310, 49–55. https://doi.org/10.1016/j.chemgeo.2012.03.008.

Flores, R.M., Rice, C.A., Stricker, G.D., Warden, A., Ellis, M.S., 2008. Methanogenic pathways of coal-bed gas in the Powder River Basin, United States: the geologic factor. Int. J. Coal Geol. 76 (1–2), 52–75. https://doi.org/10.1016/j.coal.2008.02.005.

Fu, H.J., Tang, D.Z., Pan, Z.J., Yan, D.T., Wang, G., 2019. A study of hydrogeology and its effect on coalbed methane enrichment in the southern Junggar Basin. AAPG (Am. Assoc. Pet. Geol.) Bull. 103 (1), 189–213. https://doi.org/10.1306/06071817190.

Fu, H.J., Yan, D.T., Yang, S.G., Wang, X.M., Pan, Z.J., 2021. A study of the gas-water characteristics and their implications for the CBM accumulation modes in the southern Junggar Basin, China. AAPG (Am. Assoc. Pet. Geol.) Bull. 105 (1), 189–221. https://doi.org/10.1306/02282018273.

Gao, L., Brassell, S.C., Mastalerz, M., Schimmelmann, A., 2013. Microbial degradation of sedimentary organic matter associated with shale gas and coalbed methane in eastern Illinois Basin (Indiana), USA. Int. J. Coal Geol. 107, 152–164. https://doi.org/10.1016/j.coal.2012.09.002.

Guo, Z.X., Yang, Y.T., Ren, Y., Wang, Z.Q., Feng, Z.G., Chen, L., Tang, Z.P., 2022. Emplacement and episodic denudation of the basement granites from the southern Jiergalangtu Sag in the Erlian Basin and its tectonic implications. Earth Sci. Front. 30 (2), 259–271. https://doi.org/10.13745/j.esf.sf.2022.2.58 (in Chinese).

Golding, S.D., Boreham, C.J., Esterle, J.S., 2013. Stable isotope geochemistry of coal bed and shale gas and related production waters: a review. Int. J. Coal Geol. 120, 24–40. https://doi.org/10.1016/j.coal.2013.09.001.

Hamilton, S.K., Golding, S.D., Baublys, K.A., Esterle, J.S., 2014. Stable isotopic and molecular composition of desorbed coal seam gases from the Walloon Subgroup, eastern Surat Basin, Australia. Int. J. Coal Geol. 122, 21–36. https://doi.org/10.1016/j.coal.2013.12.003.

Hamilton, S.K., Esterle, J.S., Golding, S.D., 2012. Geological interpretation of gas content trends, Walloon Subgroup, eastern Surat Basin, Queensland, Australia. Int. J. Coal Geol. 101, 21–35. https://doi.org/10.1016/j.coal.2012.07.001.

Kotarba, M.J., 2001. Composition and origin of coalbed gases in the Upper Silesian and Lublin basins, Poland. Org. Geochem. 32 (1), 163–180. https://doi.org/10.1016/S0146-6380(00)00134-0.

Kvenvolden, K.A., 1995. A review of the geochemistry of methane in natural gas hydrate. Org. Geochem. 23 (11), 997–1008. https://doi.org/10.1016/0146-6380(96)00002-2.

Li, Y.G., Yao, C.P., Yang, S.G., Fu, H.J., Wang, G., Zhang, N., Liu, Z., 2021a. Study on origin and accumulation mechanism of coalbed methane in Miquan Area of southern margin of Zhunggar Basin. Coal Sci. Technol. 49 (4), 220–226. https://doi.org/10.13199/j.cnki.cst.2021.04.027 (in Chinese).

Li, Y.B., Zeng, L., Hu, W.Q., Chen, X., Ma, L.T., Liu, C., Huang, Y., Qiao, F., 2021b. Geochemical characteristics and genesis of coalbed methane in Baode area. Coal Geol. Explor. 49 (2), 133–141. https://doi.org/10.3969/j.issn.1001-1986.2021.02.017 (in Chinese).

Liu, D.M., Zhao, Z., Cai, Y.D., Sun, F.R., 2024. Characterizing coal gas reservoirs: a multiparametric evaluation based on geological and geophysical methods. Gondwana Res. 133, 91–107. https://doi.org/10.1016/j.gr.2024.06.001.

Milkov, A.V., Etiope, G., 2018. Revised genetic diagrams for natural gases based on a global dataset of > 20,000 samples. Org. Geochem. 125, 109–120. https://doi.org/10.1016/j.orggeochem.2018.09.002.

Moore, T.A., Bowe, M., Nas, C., 2014. High heat flow effects on a coalbed methane reservoir, East Kalimantan (Borneo), Indonesia. Int. J. Coal Geol. 131, 7–31. https://doi.org/10.1016/j.coal.2014.05.012.

Ma, X.X., Hou, D.J., Wu, P., Cheng, X., Ding, W.J., Cao, L.Z., Wei, X.L., Zheng, R.H., 2023. Organic geochemistry and organic matter enrichment mechanisms of the lacustrine source rocks from a small-faulted Basin: a case study of the Bayindulan, A'er and Wuliyasitai sags in the Erlian Basin, Northern China. Geoenergy Sci. Eng. 225, 211638. https://doi.org/10.1016/j.geoen.2023.211638.

Ma, T.S., Liu, J.H., Fu, J.H., Wu, B.S., 2022. Drilling and completion technologies of coalbed methane exploitation: an overview. Int. J. Coal Sci. Technol. 9 (5), 1–31. https://doi.org/10.1007/s40789-022-00540-x.

Ma, Z.Y., Tao, S., Gao, L.C., Cui, Y., Jing, Q.H., Chen, S.D., He, W., Guo, J., Hai, L.F., 2024. Detailed characterization of microscopic pore structure in low-rank coal: a case study of zhalainuoer Coalfield. Nat. Resour. Res. 33 (5), 2261–2277. https://doi.org/10.1007/s11053-024-10355-z.

Qin, Y., Moore, T.A., Shen, J., Yang, Z., Shen, Y., Wang, G., 2017. Resources and geology of coalbed methane in China: a review. Int. Geol. Rev. 60 (5–6), 777–812. https://doi.org/10.1080/00206814.2017.1408034.

Schoell, M., 1983. Genetic characterization of natural gases. AAPG (Am. Assoc. Pet. Geol.) Bull. 67 (12), 2225–2238. https://doi.org/10.1306/AD46094A-16F7-11D7-8645000102C1865D.

Scott, A.R., Kaiser, W.R., Ayers, W.B., 1994. Thermogenic and secondary biogenic gases, San Juan Basin, Colorado and New Mexico—implications for coalbed gas producibility. AAPG (Am. Assoc. Pet. Geol.) Bull. 78 (8), 1186–1209. https://doi.org/10.1306/A25FEAA9-171B-11D7-8645000102C1865D.

Strąpoć, D., Mastalerz, M., Dawson, K., Macalady, J., Callaghan, A.V., Wawrik, B., Turich, C., Ashby, M., 2011. Biogeochemistry of microbial coal-bed methane. Annu. Rev. Earth Planet Sci. 39 (1), 617–656. https://doi.org/10.1146/annurev-earth-040610-133343.

Sun, Q.P., Wang, S.W., Tian, W.G., Sun, B., Chen, Y.J., Yang, Q., Chen, H., Yang, M.F., Qi, L., 2018. Accumulation patterns of low-rank coalbed methane gas in the Jiergalangtu Sag of the Erlian Basin. Nat. Gas. Ind. 38 (4), 59–66. https://doi.org/10.3787/j.issn.1000-0976.2018.04.007 (in Chinese).

Schimmelmann, A., Sessions, A.L., Mastalerz, M., 2006. Hydrogen isotopic (D/H) composition of organic matter during diagenesis and thermal maturation. Annu. Rev. Earth Planet Sci. 34, 501–533. https://doi.org/10.1146/annurev.earth.34.031405.125011.

Tang, S.L., Tang, D.Z., Tao, S., Sun, B., Zhang, A.B., Zhang, T.Y., Pu, Y.F., Zhi, Y.H., 2022. CO_2-enriched CBM accumulation mechanism for low-rank coal in the southern Junggar Basin, China. Int. J. Coal Geol. 253, 103955. https://doi.org/10.1016/j.coal.2022.103955.

Tang, Y., Gu, F., Wu, X., Ye, H., Yu, Y., Zhong, M., 2018. Coalbed methane accumulation conditions and enrichment models of Walloon coal measure in the Surat Basin, Australia. Nat. Gas. Ind. 5 (3), 235–244. https://doi.org/10.1016/j.ngib.2017.11.007.

Tao, S., Chen, S.D., Pan, Z.J., 2019a. Current status, challenges, and policy suggestions for coalbed methane industry development in China: a review. Energy Sci. Eng. 7 (4), 1059–1074. https://doi.org/10.1002/ese3.358.

Tao, S., Pan, Z.J., Tang, S.L., Chen, S.D., 2019b. Current status and geological conditions for the applicability of CBM drilling technologies in China: a review. Int. J. Coal Geol. 202, 95–108. https://doi.org/10.1016/j.coal.2018.11.020.

Tao, J.J., Shen, J., Wang, J.Y., Li, Y.P., Li, C., 2019c. Genetic types and exploration prospect of coalbed methane in Jiergalangtu depression, Erlian Basin. Geol. J. China Univ. 25 (2), 295–301. https://doi.org/10.16108/j.issn1006-7493.2018080 (in Chinese).

Tao, S., Chen, S.D., Tang, D.Z., Zhao, X., Xu, H., Li, S., 2018. Material composition, pore structure and adsorption capacity of low-rank coals around the first coalification jump: a case of eastern Junggar Basin, China. Fuel 211, 804–815. https://doi.org/10.1016/j.fuel.2017.09.087.

Tao, S., Tang, D.Z., Xu, H., Li, S., Geng, Y.G., Zhao, J.L., Wu, S., Meng, Q., Kou, X., Yang, S.Y., 2017. Fluid velocity sensitivity of coal reservoir and its effect on coalbed methane well productivity: a case of Baode Block, northeastern Ordos Basin, China. J. Petrol. Sci. Eng. 152, 229–237. https://doi.org/10.1016/j.petrol.2017.02.021.

Tao, S., Wang, Y.B., Tang, D.Z., Xu, H., Lv, Y.M., He, W., Li, Y., 2012. Dynamic variation effects of coal permeability during the coalbed methane development process in the Qinshui Basin, China. Int. J. Coal Geol. 93, 16–22. https://doi.org/10.1016/j.coal.2012.01.006.

Tian, W.G., Tang, D.Z., Wang, Z.L., Sun, B., 2012. Origin of coalbed methane in Baode, northeastern Ordos Basin. Geol. J. China Univ. 18 (3), 479–484. https://doi.org/10.16108/j.issn1006-7493.2012.03.020 (in Chinese).

Vinson, D.S., Blair, N.E., Martini, A.M., Larter, S., Orem, W.H., McIntosh, J.C., 2017. Microbial methane from in situ biodegradation of coal and shale: a review and reevaluation of hydrogen and carbon isotope signatures. Chem. Geol. 453, 128–145. https://doi.org/10.1016/j.chemgeo.2017.01.027.

Wang, Q., Xu, H., Tang, D.Z., Yang, S.G., Wang, G., Ren, P.F., Dong, W.Y., Guo, J.Z., 2022. Indication of origin and distribution of coalbed gas from stable isotopes of gas and coproduced water in Fukang area of Junggar Basin, China. AAPG (Am. Assoc. Pet. Geol.) Bull. 106 (2), 387–407. https://doi.org/10.1306/09152120028.

Whiticar, M.J., 1999. Carbon and hydrogen isotope systematics of bacterial formation and oxidation of methane. Chem. Geol. 161 (1), 291–314. https://doi.org/10.1016/S0009-2541(99)00092-3.

Whiticar, M.J., Faber, E., Schoell, M., 1986. Biogenic methane formation in marine and freshwater environments: CO_2 reduction vs. acetate fermentation—isotope evidence. Geochem. Cosmochim. Acta 50 (5), 693–709. https://doi.org/10.1016/0016-7037(86)90346-7.

Waples, D.W., Marzi, R.W., 1998. The universality of the relationship between vitrinite reflectance and transformation ratio. Org. Geochem. 28 (6), 383–388. https://doi.org/10.1016/S0146-6380(97)00122-8.

Wu, Y.N., Tao, S., Bi, C.Q., Tang, S.L., Men, X.Y., 2023. Pore-fracture and permeability heterogeneity of different macrolithotypes of medium-rank coals in Jixi Basin, China. Geoenergy Sci. Eng. 231, 212395. https://doi.org/10.1016/j.geoen.2023.212395.

Xu, H., Tang, D.Z., Zhao, J.L., Tao, S., Li, S., Fang, Y., 2015. Geologic controls of the production of coalbed methane in the Hancheng area, southeastern Ordos Basin. J. Nat. Gas Sci. Eng. 26, 156–162. https://doi.org/10.1016/j.jngse.2015.06.018.

Xu, F.Y., Xiao, Z.H., Chen, D., Yan, X., Wu, N., Li, X.F., Miao, Y.N., 2019. Current status and development direction of coalbed methane exploration technology in China. Coal Sci. Technol. 47 (10), 205–215. https://doi.org/10.13199/j.cnki.cst.2019.10.027 (in Chinese).

Ye, J.C., Tao, S., Zhao, S.P., Li, S., Chen, S.D., Cui, Y., 2022. Characteristics of methane adsorption/desorption heat and energy with respect to coal rank. J. Nat. Gas Sci. Eng. 99, 104445. https://doi.org/10.1016/j.jngse.2022.104445.

Zhang, B., Zhang, Y.F., Zhao, S.P., He, W., Tao, S., Pan, Z.J., Cui, Y., 2022. Coalbed methane desorption characteristics controlled by coalification and its implication on gas co-production from multiple coal seams. Front. Earth Sci. 17 (1), 121–134. https://doi.org/10.1007/s11707-022-0974-y.

Zhou, Z., Ballentine, C.J., Kipfer, R., Schoell, M., Thibodeaux, S., 2005. Noble gas tracing of groundwater/coalbed methane interaction in the San Juan Basin, USA. Geochem. Cosmochim. Acta 69 (23), 5413–5428. https://doi.org/10.1016/j.gca.2005.06.027.

Zhang, Y., Li, S., Tang, D.Z., Zhao, X.L., Ye, J.C., 2020. Structure- and hydrology-controlled isotopic coupling and heterogeneity of coalbed gases and co-produced water in the Yanchuannan block, southeastern Ordos Basin. Int. J. Coal Geol. 232, 103626. https://doi.org/10.1016/j.coal.2020.103626.

Zhang, B., Tao, S., Sun, B., Tang, S.L., Chen, S.D., Wen, Y.J., Ye, J.C., 2024. Genesis and accumulation mechanism of external gas in deep coal seams of the Baijiahai Uplift, Junggar Basin, China. Int. J. Coal Geol. 286, 104506. https://doi.org/10.1016/j.coal.2024.104506.

Zhang, C.L., Wang, P.Z., Wang, E.Y., Chen, D.P., Li, C., 2023. Characteristics of coal resources in China and statistical analysis and preventive measures for coal mine accidents. Int. J.Coal Sci. Technol. 10 (2), 45–57. https://doi.org/10.1007/s40789-023-00582-9.